From DEPARTMENT OF NEUROSCIENCE
Karolinska Institutet, Stockholm, Sweden

# MEMBRANE MECHANISMS DURING EXO- AND ENDOCYTOSIS IN EXCITABLE CELLS

Gianvito Arpino


Karolinska Institutet

Stockholm 2020

Published by Karolinska Institutet.
Printed by Eprint AB 2020

ISBN 978-91-7831-773-8

# Membrane mechanisms during exo- and endocytosis in excitable cells

**THESIS FOR DOCTORAL DEGREE (Ph.D.)**

Public defence: Thursday 7th of May 2020, 10 am

Lecture Hall Charles; Tomtebodavägen 18 A, Solna

By


## Gianvito Arpino

*Principal Supervisor:*
Professor Oleg Shupliakov
Department of Neuroscience

*Co-supervisor(s):*
Professor Ling-Gang Wu
National Institute of Health
National Institute of Neurological Disorders and Strokes
Synaptic Transmission Section

Professor Lennart Brodin
Karolinska Institutet
Department of Neuroscience

*Opponent:*
Associate Professor Richard Lundmark
Umeå Universitet
Department of Integrative Medical Biosciences

*Examination Board:*
Professor Per. O. Ljungdahl
Stockholm Universitet
Department of Molecular Biosciences
The Wenner-Gren Institute

Associate Professor Ilaria Testa
KTH Royal Institute of Technology
Science for Life Laboratory

Associate Professor Mia Lindskog
Karolinska Institutet
Center for Alzheimer Research

*"La più consistente scoperta che ho fatto è che non posso più perdere tempo a fare cose che non mi va di fare"*

Cit. Jep Gambardella

# ABSTRACT

Excitable cells, like endocrine cells and neurons release hormones and transmitters through exocytosis to mediate many important functions, such as stress responses, immune responses, control of blood glucose, and synaptic transmission that mediates communication between neurons in the brain. This process relies on delicate endocytic mechanisms, to retrieve vesicular membranes and proteins previously fused at the plasma membrane and thus maintains the ability of exocytosis for excitable cells.

Upon exocytosis, vesicle fusion with the plasma membrane generates an Ω-shape membrane profile with a narrow fusion pore (< ~5 nm), through which the vesicular content is released. For decades, it has been thought that the narrow pore of the Ω-profile either dilates till the Ω-profile flattens to facilitate content release (full-collapse) or closes to limit content release (kiss-and-run). Using a combination of confocal, super-resolution STED and electron microscopy, we found that this classical view needs to be modified significantly. We observed that the fusion pore may expand, constrict and/or close at different rates to regulate content release and that its size may vary between 0 and 490 nm. The cytoskeletal F-actin facilitates fusion pore opening. The merge between fused vesicles and the plasma membrane is not via the full-collapse fusion mode, but via Ω-profile shrinking while maintaining the Ω-shape (Ω-shrink fusion mode). F-actin provides sufficient membrane tension to facilitate Ω-shrink fusion in neuroendocrine chromaffin cells, and to facilitate vesicle merging at lamprey giant synapses. Thus, facilitation of vesicle merging by F-actin may be applicable to many secretory cells and synapses. Unlike the classical view that full-collapse and kiss-and-run facilitate and limit release, respectively, facilitation is mediated by shrink-fusion with a large non-dilating pore, whereas during inhibition, by enlarge-fusion that enlarges the Ω-profile, a small pore is maintained. Shrink and enlarge-fusion may account for diverse hormone and transmitter release kinetics observed in secretory cells.

Clathrin-mediated endocytosis (CME), the most common form of endocytosis, is considered to retrieve vesicles from the flat plasma membrane. With conventional and platinum replica electron microscopy (EM), we found that clathrin-coated pits prefer to be localized at the bulk invagination of the plasma membrane instead of the flat plasma membrane. Using super-resolution STED microscopy, we observed for the first-time direct budding of vesicles from bulk membrane invagination. These results suggest that bulk membrane invaginations are a major platform for mediating clathrin-dependent

endocytosis, calling for modification of the current view that clathrin-mediated endocytosis mostly originated from the flat plasma membrane.

In summary, the studies described here improve our understanding of the regulation of hormone and transmitter release as well as endocytosis.

# LIST OF SCIENTIFIC PAPERS

I. GIANVITO ARPINO, Lihao Ge, Shin Wonchul, Seth Villareal, Uri Ashery, Agila Somasundaram, Justin Taraska, Oleg Shupliakov, Ling-Gang Wu. Bulk invagination at the plasma membrane is the primary site for clathrin-mediated endocytosis. Manuscript.

II. Peter J. Wen*, Staffan Grenklo*, GIANVITO ARPINO, Xinyu Tan, Hsien-Shun Liao, Johanna Heureaux, Shi-Yong Peng, Hsueh-Cheng Chiang, Edaeni Hamid, Wei-Dong Zhao, Wonchul Shin, Tuomas Näreoja, Emma Evergreen, Yinghui Jin, Roger Karlsson, Steven N. Ebert, Albert Jin, Allen P. Liu, Oleg Shupliakov and Ling-Gang Wu. Actin dynamics provides membrane tension to merge fusing vesicles into the plasma membrane. Nature Commun, 2016. 7. p. 12604.

III. Wonchul Shin, Lihao Ge, GIANVITO ARPINO, Seth Villareal, Edaeni Hamid, Huisheng Liu, Wei-Dong Zhao, Peter J. Wen P, Hsueh-Chiang and Ling-Gang Wu . Visualization of Membrane Pore in Live Cells Reveals a Dynamic-Pore Theory Governing Fusion and Endocytosis. Cell, 2018, 4: p. 934.

IV. Wonchul Shin*, GIANVITO ARPINO*, Sathish Thiyagarajan*, Rui Su*, Liaho Ge*, McDargh Zachary, Xiaoli Guo, Lisi Wei, Oleg Shupliakov, Albert Jin A, Ben O'Shaughnessy B, Ling-Gang Wu. Vesicle Shrinking and Enlargement Play Opposing Roles in the Release of Exocytotic Contents. Cell Reports, 2020, 30. p. 421

* Contributed equally to this work.

# PUBLISHED REPORTS

I. Vesicle Shrinking and Enlargement Play Opposing Roles in the Release of Exocytotic Contents. Shin W., ARPINO G., Thiyagarajan S., Su R., Ge L., McDargh Z., Guo X, Wei L, Shupliakov O., Jin A., O'Shaughnessy B., and Ling-Gang Wu. Biophysical Journal., 2020, Vol. 118, Issue 3, p399a.

II. ARPINO G., Shin W., Shupliakov O., Wu LG. Vesicle Structural Changes Control Content Release of Transmitters and Hormones. Microscopy and Microanalysis, 2019, 25: p. 1172.

III. ARPINO G., Wu LG, Bleck C. Ultrastructural preservation and improved visualization of membranes in primary bovine chromaffin cells. Capturing Dynamic Processes with High Pressure Freezing. Application Note for HPF EM ice. Leica. 21st October 2019.

IV. ARPINO G., Näreoja T., Sopova E., Shupliakov O..Actin-dependent mechanisms during vesicle fusion link exo- and endocytosis in synapses. Life Sciences. European Microscopy Congress 2016: Proceedings. Life Sciences Cell functional exploration.

V. Villareal S., ARPINO G., Shin W., Wu LG. Characteristics of Bulk

Endocytosis within Chromaffin Cells. Biophysical journal. , 2018, Vol.114 (3), p. 104a.

# CONTENTS

# LIST OF ABBREVIATIONS

| | |
|---|---|
| **ATPγS** | **Adenosine-5'-triphosphate** |
| **Ccp** | **Clathrin coated pit** |
| **Cyt D** | **Cytochalasin D** |
| **Ccv** | **Clathrin coated vesicle** |
| **EM** | **Electron microscopy** |
| **GTP** | **Guanosine-5'-triphosphate** |
| **GTPγS** | **Guanosine-5'-triphosphate** |
| **Lat A** | **Latrunculin A** |
| **mTurq** | **mTurquoise** |
| **PH** | **Pleckstrin homology domain** |
| **$PH_G$** | **PH-mNeonGreen** |
| **$PI(4,5)P_2$** | **Phosphoinositol-(4-5)-bis-phosphate** |
| **PM** | **Plasma membrane** |
| **$ddH_2O$** | **Double distilled water** |
| **STED** | **Stimulated emission depletion** |

# 1 INTRODUCTION

## 1.1 Excitable cell

All cells have a resting potential, represented by the imbalance of electrical charge across the plasma membrane between the interior of the cell and its surroundings. The resting potential in excitable cells is around -70 mV. Excitable cells have the characteristic to be electrically excitable and consequently generate action potentials. Neurons, muscle cells, and endocrine cells, like insulin-releasing pancreatic β-cells and catecholamine-releasing chromaffin cells, are excitable cells (Brandt, Hagiwara et al. 1976, Jacobson and Philipson 2007).

## 1.2 The cycle of a secretory vesicle in excitable cells

In neurons and endocrine cells, action potentials open voltage-dependent calcium channels. The influx of calcium triggers vesicle fusion with the plasma membrane and secretion of vesicular contents, including hormones and transmitters. Hormone and transmitter release mediates many crucial biological processes (Sudhof 2004), such as synaptic transmission essential for our brain functions, secretion of insulin that regulates the blood glucose level critically related to diabetes (Rorsman and Braun 2013), and secretion of serotonin in the regulation of mood and cognition (Jenkins, Nguyen et al. 2016). These examples represent only a small subset of all the substances released in our body through exocytosis. Excitable cells can sustain high rates of exocytosis without depleting their vesicle supply. This feature relies on delicate endocytic mechanisms that allow the cells to retrieve vesicular membranes and proteins previously fused at the plasma membrane. In this work, I focused on membrane mechanisms during exo- and endocytosis (Fig. 1).

## 1.3 Exocytosis

Exocytosis is an active process adopted by the cell to transport material within the cell into the extracellular environment. Two mechanisms of exocytosis are thought to operate in secretory cells: the full-collapse mode, in which a vesicle fuses with the plasma membrane, opens a fusion pore, followed by dilation of the pore until flattening, which facilitates content release; and the “kiss-and-run” mode, where the fusion pore opens and closes transiently without vesicle collapse (Wu, Hamid et al. 2014).

### 1.3.1 Full-collapse mode and kiss-and-run

The first hint of full-collapse fusion came from electron microscopy studies at the frog neuromuscular junction (NMJ) in 1981. Heuser and Reese observed pockets and curvatures with the same size as a synaptic vesicle at the active zone (Heuser and Reese 1981) (Fig. 1a) that was later been interpreted as full-collapse of vesicles. Several indirect lines of evidence are consistent with this fusion mode. Recordings of membrane capacitance in secretory cells in the cell-attached configuration showed that the capacitance up-step caused by single vesicle fusion was followed by an increase of pore conductance that may indicate pore expansion beyond ~5 nm (Alvarez de Toledo, Fernandez-Chacon et al. 1993, Albillos, Dernick et al. 1997, Taraska, Perrais et al. 2003, He, Wu et al. 2006). Consistent with pore expansion, catecholamine release measured by amperometry revealed rapid content release (Albillos, Dernick et al. 1997). Based on these results, it has been suggested that the role of full-collapse fusion of vesicles in secretory cells is to permit fast and complete release of the vesicular content through fusion pore expansion. Live-cell evidence of full-collapse fusion was recently showed in chromaffin cells. Using super-resolution STED microscopy, fluorescent proteins and impermeable dyes, it has been possible to visualize the transition from hemi-fusion to full-fusion in live cells. This technique opens the doors to new approaches to study pore dynamics (Zhao, Hamid et al. 2016) and might help to elucidate the full-collapse mode.

Kiss-and-run mechanism was proposed based on EM observation of the Ω-shape intermediate at the NMJ (Ceccarelli, Hurlbut et al. 1973) (Fig. 1b). However, EM alone was not sufficient to make a compelling case, because it was not possible to predict whether the Ω-profile was a structure *en route* towards full-collapse or fusion pore closure (Alabi and Tsien 2013). More convincing evidence was put forth in chromaffin cells and PC12 by the observation of capacitance flickers accompanied by amperometric recordings. Amperometry gives direct information about the release process. These data showed a stand-alone foot of the signal, implying partial transmitter release (Alvarez de Toledo, Fernandez-Chacon et al. 1993, Fesce, Grohovaz et al. 1994, Albillos, Dernick et al. 1997). Kiss-and-run is generally considered the mechanism to limit vesicular release, given its narrow pore, but it may also ensure a fast and complete vesicular release by leading to opening of a large pore (Ales, Tabares et al. 1999). Interestingly, this mechanism might be interpreted as a way to save energy. Recent studies in live chromaffin cells showed post-fusion structural changes of the Ω-profile. The fusion-generated Ω-profile can be detected with confocal or super-resolution STED microscopy. The structural changes of the Ω-profile were detected in cells incubated with two different membrane impermeable dyes.

This study established a new exo-endocytosis model, in which the Ω-profile changes in seven patterns by fusion pore closure and size transformation. The model redefines both full-collapse and kiss-and-run. The fusion mode that allows for the merge of the vesicle membrane with the plasma membrane is not truly a full-collapse mode, but a mode called Ω-shrink, in which the fusion with the plasma membrane occurs by Ω-profile shrinking and not by pore dilation until flattening. Kiss-and-run instead, was redefined as close fusion, a mode that generate vesicles with different sizes by shrinking or enlarging the Ω-profile before closure (Chiang, Shin et al. 2014). The live approaches above represent an excellent tool to study fusion processes and pore dynamics (Chiang, Shin et al. 2014, Zhao, Hamid et al. 2016). In the near future, the combination of these imaging techniques with labelling of vesicular contents [e.g. false fluorescent neurotransmitters (Evanko 2009), neuropeptide Y-GFP] and protein knockdown may promise to improve our understanding of exocytosis mechanisms and help to determine the efficiency of vesicular cargo release.

## 1.4 Endocytosis

Endocytosis is the process of active transport of substances into the cell, and it consists of the formation of plasma membrane invaginations forming pockets that eventually bud off. The plasma membrane portions retrieved are reused to create new vesicles for reuse in exocytosis. There are three mode of endocytosis in excitable cells: clathrin-mediated endocytosis, a mechanism that recycles vesicles via the coating protein clathrin; kiss-and-run (the same as during exocytosis); and bulk endocytosis, characterized by retrieval of large portion of membranes (Fig. 1c-e) (Wu, Hamid et al. 2014)

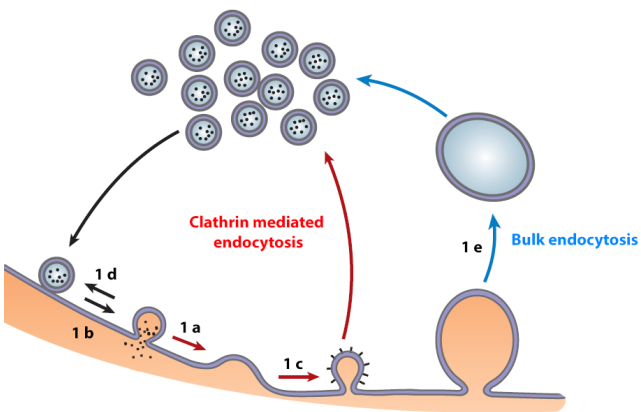


Figure 1: The schematic draw shows modes of exocytosis and endocytosis in secretory cells. Three modes of exocytosis: full-collapse (1a), kiss-and-run (1b) followed by three modes of endocytosis: clathrin mediated endocytosis (1c), kiss-and-run (1d) and bulk endocytosis (1e). Figure adapted from (Wu, Hamid et al. 2014)

### 1.4.1 Clathrin-mediated endocytosis

During mild stimulation in excitable cells, single vesicles are formed directly from the plasma membrane (Fig. 1c). This mechanism was first observed by electron microscopy in the NMJ, where coated vesicles represented the actual mechanism to retrieve synaptic vesicle membrane from the plasma membrane (Heuser and Reese 1973). A couple of years later, coated vesicles were purified, and it was discovered that the coat was made of clathrin, a protein that surrounds the vesicle with an icosahedral arrangement (Pearse 1975, Pearse 1976). Since that finding, over 50 proteins have been shown to be part of the clathrin-mediated endocytosis machinery (Kaksonen and Roux 2018) and numerous studies have aimed to elucidate the importance of this mechanism. For example, disruption of a specific domain of the fission protein dynamin and knock-down of the clathrin adaptor protein AP180 were found to cause impairment of endocytosis, suggesting the involvement of dynamin and AP180 in endocytosis (Shupliakov, Low et al. 1997, Zhang, Koh et al. 1998). In other studies, using a large nerve terminal, the Calyx of Held, cell-attached capacitance recording revealed capacitance down-steps reflecting classical endocytosis, because the absence of a preceding up step indicated that it did not reflect kiss-and-run and its size was too small to be caused by bulk endocytosis (He, Wu et al. 2006). The role of clathrin in endocytosis was also demonstrated in *clathrin heavy chain* (*chc*) mutants in *Drosophila melanogaster* in combination with chc photoinactivation. The data showed a decline in neurotransmitter release during intense stimulation and that membrane recycled could not participate in the second round of release. Moreover, in cells lacking chc, a different form of membrane retrieval, takes over, suggesting that the inactivation of clathrin heavy chain prevents vesicle recycling, but not bulk membrane uptake (Kasprowicz, Kuenen et al. 2008). These are just a few of the many pieces of evidence demonstrating the existence of clathrin-mediated endocytosis in secretory cells and its importance in endocytosis.

At the ultrastructural level, based on EM observations at the NMJ, it was proposed that clathrin-coated vesicles are pinched off from the plasma membrane, followed by clathrin uncoating, and eventual fusion with endosome-like structures. The latter were proposed to act as the precursor for the genesis of new synaptic vesicles (Heuser and Reese 1973, Miller and Heuser 1984, Watanabe, Trimbuch et al. 2014). The model considered two budding steps, in which a clathrin-coated vesicle buds off from the plasma membrane first, and then from the endosome (Fig. 2a). With the use of lysed nerve terminal and nerve terminal membrane sub-fractions, a different model was proposed, in which synaptic vesicles are generated by a single budding step, either from the flat plasma membrane or

from endosome-like structures (Fig. 2b) (Takei, Mundigl et al. 1996, Watanabe, Trimbuch et al. 2014). These models were proposed based on EM, but not from direct observations in live cells. Thus, the key evidence showing the dynamic process of these budding processes is still missing. The visualization of the dynamic structural changes in live cells will ultimately provide the detailed description of these budding processes and thus prove or disapprove these models.

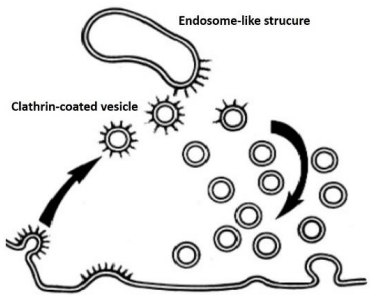


Figure 2 - a) Vesicle generation in two budding steps. Clathrin-coated vesicles fuse and bud off from an existing endosome-like structure. Figure adapted from (Miller and Heuser 1984)

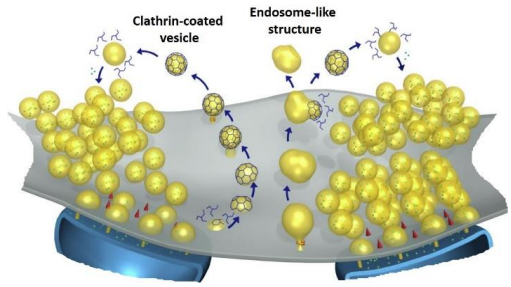


Figure 2 - b) Vesicle generation in one budding step. Vesicles generated either from flat plasma membrane (left) or from endosome-like structures (right). Figure adapted from (Kononenko and Haucke 2015)

### 1.4.2 Bulk endocytosis

During increased neuronal activity, a large number of vesicles fuse with the plasma membrane. To maintain the equilibrium and sustain high rates of transmission, cells have developed bulk endocytosis, formation of large endosome-like structures from the plasma membrane, to retrieve vesicle membranes (Clayton, Evans et al. 2008) (Fig. 1e). Following bulk endocytosis, vesicles bud off from large endosome-like structures. Bulk endocytosis was first observed with EM at the NMJ after intense stimulation (Heuser and Reese 1973). The kinetics of bulk endocytosis was described using whole-cell capacitance recordings at the giant calyx of Held. The recordings revealed large capacitance jumps that reflect fission step of invaginations much larger than a regular vesicle (Wu and Wu 2007). Since large bulk invaginations at the plasma membrane are considered the precursor of the cytosolic endosome-like structure, it was initially proposed that clathrin-coated pits can also be generated from bulk invaginations. However, in this early study, the key evidence supporting the proposal, a bulk invagination with clathrin-coated pits, was only shown in low quality images, in which it is hard to establish whether the bulk invagination was connected to the plasma membrane or not (Takei, Mundigl et al. 1996). Direct electron

microscopic evidence supporting clathrin-coated vesicle generation from bulk membrane invagination under control conditions is needed to support the proposal that clathrin-coated pits can be generated from bulk invaginations at the plasma membrane. Furthermore, whether clathrin-coated pits can be pinched off directly from bulk membrane invaginations remains unclear.

## 1.5 The roles of actin in excitable cells

Actin cytoskeleton plays a crucial role in many physiological processes in eukaryotic cells, such as maintaining cellular shape, motility, trafficking, and communication. Its specific deformations and movements are a result of a highly regulated assembly/disassembly that explains its dynamics. Actin filaments have been clearly visualized in excitable cells, using "quick-freeze, deep-etch" electron microscopy. It has been demonstrated that a network of long filaments arise from the plasma membrane and interconnect with shorter filament associated with vesicles (Landis, Hall et al. 1988). In neurons, for example, decoration of actin filaments with S1 myosin sub-fragments showed their association with the plasma membrane (Fifkova and Delay 1982) and platinum replica electron microscopy showed that actin cytoskeleton is made of actin filaments (Korobova and Svitkina 2010). Actin was localized at the active zones of synapses and around synaptic vesicle clusters. Experiments with fluorescent actin in rat CNS neurons attempted to address its role in the vesicle cycle (Sankaranarayanan, Atluri et al. 2003, Li, Bai et al. 2010). Early studies in human platelets and chromaffin cells showed an association of the actin network with some organelles (Nakata and Hirokawa 1987) and a possible role in exocytosis (Aunis and Bader 1988). Other studies in budding yeast supported the idea of actin´s involvement in endocytosis. Light microscopy has demonstrated the participation of actin in endocytosis in mammalian cells (Smythe and Ayscough 2006) suggesting that actin plays many different roles in exo- and endocytosis in excitable cells. In the following, I summarize its main functions and the unsettled issues.

## 1.6 Actin dynamics is required for exocytosis

In small synapses, the general trend is that inhibition of actin polymerization facilitates exocytosis. For example, latrunculin A, which prevents polymerization and thus promotes actin filament disassembly, increases neurotransmitter release (Morales, Colicos et al. 2000). A similar effect was found in mice lacking the actin binding protein profilin 2. Actin polymerization is blocked in response to depolarization, which increases synaptic vesicle

release (Pilo Boyl, Di Nardo et al. 2007). These data suggest that actin filaments act as a barrier to prevent exocytosis. However, this suggestion is inconsistent with the recent findings in ADF (actin depolymerizing factor) and cofilin 1 mutant mice. The function of these two proteins is to depolymerize actin filaments, therefore ADF/cofilin 1 mutations might increase the rigidity of the synaptic actin cytoskeleton. Inactivation of ADF/cofilin resulted in an increase of exocytosis (Wolf, Zimmermann et al. 2015). These apparently contradictory findings may imply that actin dynamics is needed for the synapse to carry out its exocytotic function. In chromaffin cells, instead, the barrier model has been supported by fluorescence and electron microscopy studies. The disruption of cortical actin by the treatment with phorbol ester increases the number of secretory vesicles that approach the plasma membrane and increases the initial rate of catecholamine release (Vitale, Seward et al. 1995). The evidence discussed above represent a minimal part of the studies that have explored the role of actin in excitable cells, with a common target, the exocytosis of multiple vesicles. The single fusion exocytic event was revealed for the first time by patch amperometry in 1997 (Albillos, Dernick et al. 1997), giving an important contribution to the field. Amperometry signals imply that actin is involved in the regulation of fusion pore expansion (Trouillon and Ewing 2014). However, direct visualization of fusion pore expansion is needed to verify this implication.

### 1.6.1 Actin contribution to endocytosis

Following exocytosis, endocytosis retrieves vesicle membrane and proteins, which form new vesicles to sustain the activity of exocytosis. Several studies in non-neuronal models established that actin plays a role in endocytosis (Engqvist-Goldstein and Drubin 2003). Despite this, its role in mammalian cells is rather controversial. Studies in giant reticulospinal axons in lamprey showed that, after stimulation there is a rearrangement of the network of actin filaments formed at the periactive zone. This network is associated with clathrin-coated pits at the plasma membrane and with uncoated vesicles near the vesicle cluster. Perturbation of actin with the catalytic subunit of C2 toxin from *Clostridium botulinum*, induced accumulation of clathrin coated pits at the plasma membrane and caused a reduction of the vesicle pool size (Shupliakov, Bloom et al. 2002). However, other studies in the same model blocking actin polymerization with latrunculin A, did not disrupt the pool of vesicles or endocytosis detected with FM1-43 uptake (Bleckert, Photowala et al. 2012). Additionally, stabilization of F-actin with phalloidin, reduced FM1-43 uptake and exocytosis to a similar extent, but with a stronger effect on exocytosis than endocytosis (Bleckert, Photowala et al. 2012). At the frog NMJ, a similarly controversial effect was

observed. Latrunculin A reduced FM1-43 uptake that may suggest inhibition of endocytosis, whereas perturbation of actin by cytochalasin D did not affect FM1-43 uptake or release (Richards, Rizzoli et al. 2004). In small mammalian synapses, latrunculin A was applied to the culture and cells were stimulated with a single stimulus, rapidly frozen and observed by EM. Actin perturbation blocked ultrafast endocytosis (Watanabe, Rost et al. 2013), contrasting with the lack of effect of action potential trains previously reported by Ryan and colleagues (Sankaranarayanan, Atluri et al. 2003). The recent results may be consistent with later studies in lamprey (Bleckert, Photowala et al. 2012), suggesting that actin's role is most evident after a single stimulus. In summary, the use of pharmacological blockers was not sufficient to clarify the role of actin in endocytosis. Consequently, a gene knockout approach has been recently used to elucidate actin's endocytic role in mammalian cells. Capacitance measurements at the calyx of Held in β-actin or γ-actin knockout mice showed that actin is involved in all kinetically distinct forms of synaptic endocytosis presumably to provide mechanical force to endocytic profiles (Wu, Lee et al. 2016). Consistent with the calyx data, ultrastructural data in β-actin knockout hippocampal synapses, showed a reduction of clathrin-coated pits and inhibition of bulk endocytosis (Wu, Lee et al. 2016), confirming its role in the endocytic mechanisms. Thus, emerging data suggests that actin is required for all forms of endocytosis. However, additional evidence in live cells will be required to describe how actin provides forces to mediate endocytosis. Ultimately, these findings could help to clarify the discrepancy presented in the different models and create a unified vision regarding how actin is involved in mediating endocytosis.

### 1.6.2 Actin's role in single vesicle fusion

Vesicles fuse with the plasma membrane and form an Ω-shaped membrane profile with a pore allowing for release of transmitters and hormones from the vesicular lumen to the extracellular space. Fusion pores are highly dynamic structures. They can open, expand, shrink, merge or close depending on their vesicle size (Klyachko and Jackson 2002), composition of lipids and proteins (Chernomordik and Kozlov 2008), and membrane tension (Kozlov and Chernomordik 2015). How the fusion-generated Ω-profile merge into the plasma membrane has been studied in secretory cells (*Xenopus oocytes* and lacrimal acinar cells) containing large vesicles (~100-500 μm), where vesicle fusion can take tens of seconds to occur (Sokac, Co et al. 2003, Nightingale, White et al. 2011). It has been suggested the F-actin might coat the Ω-shaped profile to prevent the collapse of the structure or provide the force to merge the Ω-profile to the plasma membrane. The hint of

a possible involvement of actin in vesicle fusion prompted the scientific community to study actin's role in excitable cells, where fusion occurs in shorter time frames (ms to sec) and smaller vesicles (30-50 nm). In chromaffin cells, for example, perturbation of actin filaments with cytochalasin D increased quantal size, a consequence of the slowed down fusion pore expansion (Gonzalez-Jamett, Momboisse et al. 2013). Using an N-WASP inhibitor and wiskostatin to inhibit actin polymerization, it was found that fusion pore expansion was restricted, thus limiting the release of transmitters (Olivares, Gonzalez-Jamett et al. 2014). Furthermore, treatment with latrunculin A in PC12 suggested the involvement of actin filaments in pore constriction (Trouillon and Ewing 2014).

Although, the studies above propose a role of actin in regulating fusion pore dynamics, the proposal needs to be verified with direct visualization of the fusion pore expansion process.

# 2 AIMS OF THE STUDY

The general aim of this thesis was to improve our understanding of the mechanisms of exo- and endocytosis, particularly regarding structural changes of membranes. Listed below are the specific goals:

I. To determine whether bulk membrane invagination serves as a platform where clathrin-dependent endocytosis takes place.

II. To investigate whether F-actin is involved in providing force to underlie the post-fusion structural change that allows for the merging of vesicles with the plasma membrane.

III. To elucidate whether F-actin is involved in providing force to regulate structural changes of the dynamic fusion pore.

IV. To determine whether fusion modes involving different structural changes of the membrane differentially control vesicular content release.

# 3 MATERIAL AND METHODS

## 3.1 Models to study exo-endo structural changes

### 3.1.1 Neuroendocrine chromaffin cells

Chromaffin cells are neuroendocrine cells found mostly in the medulla of adrenal glands, located above the kidneys. Their function is to regulate the response to stress by releasing catecholamines (adrenaline, noradrenaline) and thereby maintain respiration and blood circulation in the body (Schober, Parlato et al. 2013). Evolutionarily they are a hybrid between the endocrine and the nervous systems, and they have been used for many years to study neuronal functions (Bornstein, Ehrhart-Bornstein et al. 2012). Several exocytosis molecular mechanisms were elucidated thanks to the use of chromaffin cells (Winkler 1993, Thiele, Hannah et al. 2000). We utilized bovine chromaffin cells since they contain ~300 nm dense core vesicles. Those vesicles can be visualized by confocal and super-resolution STED microscopy at ~230 nm and 90 nm resolution, allowing the study of exo/endocytosis mechanisms. Instead, for obvious reasons, mouse chromaffin cells were preferred for gene knock-out experiments.

### 3.1.2 Reticulospinal axon in lamprey

The river Lamprey, *lampetra fluvialis* is a jawless vertebrate belonging to the superclass of Cyclostomata. Lampreys are also referred to as living fossils because of their evolutionarily conserved features (Xu, Zhu et al. 2016). In the 1970s because of their simple brain and neural network, a group of scientists from the Karolinska Institutet in Stockholm decided to use lamprey as a model to study the principles of motor control in invertebrates (Grillner 2003). Special characteristics are their large neurons and lack of myelin. For this reason, later on scientists started using synapses between these neurons to investigate molecular mechanisms of synaptic transmission (Brodin and Shupliakov 2006). The largest axons are unbranched and can reach up to 100µm in diameter. Interestingly, synapses in giant axons are clearly separated from each other with active zones and large clusters containing thousands of vesicles. An important feature of the giant reticulospinal synapse is that it contains large areas called periactive zone where synaptic vesicle recycling occurs (Gad, Low et al. 1998). The large diameter of these axons allows microinjection of drugs/compounds that can selectively affect protein-protein and protein-lipid interactions (Fig. 3).

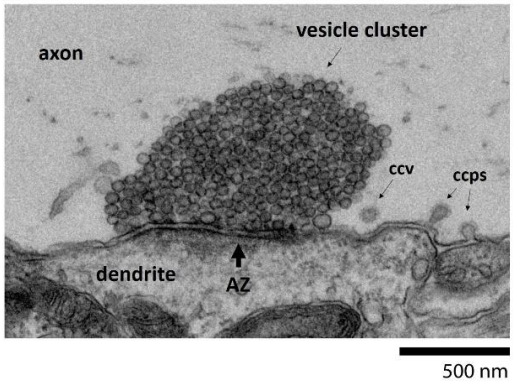


Figure 3 - Vesicle cluster of giant reticulospinal axon in lamprey. The synapse was stimulated at 5Hz for 30 min. In the micrographs clearly distinguishable (clockwise from top left): axon, vesicle cluster, clathrin-coated vesicle (ccv), clathrin-coated pits (ccps), active zone (AZ) and dendrite.

## 3.2 Chromaffin cells

### 3.2.1 Primary bovine chromaffin cell culture

Primary bovine chromaffin cells (**paper I, II, III, IV**) were prepared following the protocol from O'Connor et al. 2007 (O'Connor, Mahata et al. 2007). Fresh bovine adrenal glands derived from adult bovine (21-27 months) were obtained from a local slaughterhouse on the day of culture and immersed in a 500 ml sterile culture bottle filled with pre-chilled Lock solution buffer. The Lock solution contained (in mM): 145 NaCl, 5.4 KCl, 2.2 $Na_2HPO_4$, 0.9 $NaH_2PO_4$, 5.6 glucose, 10 Hepes and the pH adjusted at 7.3 with NaOH. After the excess fat was trimmed off the glands, each gland was perfused first with 2 ml cold Lock's solution through the portal vein to remove residual blood, then with Lock's buffer containing collagenase P (1.5 mg $ml^{-1}$, Roche), trypsin inhibitor (0.325 mg $ml^{-1}$ Sigma) and bovine albumin serum (5 mg $ml^{-1}$Sigma) and incubated at 37 °C for 20 min. The glands were cut longitudinally to expose the digested medulla. The medulla was minced in Lock's buffer and filtered through a 250 µm sterile nylon mesh. The filtrate was centrifuged at 49 g for 4 min. The supernatant was then removed, and the pellets resuspended in Lock's buffer. The process was repeated until the supernatant was clear. The final cell pellet was re-suspended in pre-warmed DMEM low glucose medium (GIBCO) supplemented with 10% fetal bovine serum.

### 3.2.2 Electroporation and plating

Cells were plated onto 25 mm diameter crystal clear German glass coverslips pre-coated with mouse Laminin over poly-D-lysin layer on both sides of the coverslips (Neuvitro), incubated at 37°C, 8% $CO_2$ and used within 3 days from after culturing. In some experiments before plating, cells were transfected by electroporation using Basic Primary

Neurons Nucleofector Kit (Lonza) program O-005 according to the manufacturer's protocol (**paper I, II, III, IV**).

### 3.2.3 Plasmids

PH-mNeonGreen (phospholipase C delta PH domain attached with mNeonGreen) construct was created by replacing the EGFP tag of PH-EGFP (obtained from Dr. Tamas Balla) with mNeonGreen (Allele Biotechnology). Clathrin-mTurquoise was purchased from Addgene **(paper I).**

### 3.2.4 STED imaging and scanning

STED images were acquired with a TCS SP8 STED 3X from Leica equipped with a 100 x 1.4 NA HC PL APO CS2 oil objective. The microscope can reach a resolution of ~ 60-90 nm. PH-mNEON green and Clathrin mTurquoise were sequentially excited with white light laser tuned at 505 nm and 442 nm respectively, STED depletion laser at 592 nm (25% of the maximum power). Their fluorescence was collected at 510-587 nm and 447-490 nm, respectively. STED images were acquired at the cell bottom with the XY (parallel to the coverslip), above the cell bottom (~2 µm) or XZ (perpendicular to the coverslip) To reconstruct 3-D structure of large invaginations, XZ images were acquired alone *y* axis every 50 nm for 2-5 mm (XZ/Y stack scanning). Images were deconvolved using Huygens software (Scientific Volume Imaging). 3D reconstruction was made using the software LAS X core **(paper I).**

### 3.2.5 Electron microscopy for cell culture

Cells on coverslips were fixed **(paper I, III, IV)** with a mixture of 2% glutaraldehyde, 2% paraformaldehyde (Electron microscope science) and 4% tannic acid (Sigma) in 0.1 M cacodylate buffer pH 7.3 for 15 min. The same fixative was used without tannic for an additional 15 min. Samples were incubated with a solution 100mM glycine in 0.1 M cacodylate for 5 min and then with just 0.1 M cacocylate buffer three times for 5 min. Subsequently, cells were post-fixed with a solution of 1% $OsO_4$ in 0.1 M Cacodylate for 60 min on ice, then rinsed in 0.1 M cacodylate three times and 1 time in $ddH_2O$, before gradually dehydration increasing solution of pure ethanol in $ddH_2O$ (25%, 50%, 70%), two times for each dilution for 5 min. Later, samples were stained with 2% uranyl acetate (Electron Microscope Science) in 70 % ethanol for 30 min followed by dehydration in (85%, 95%, and 100%) ethanol. Lastly, samples were infiltrated with increasing

concentrations (25%, 50%, 70%, 100%) of epon resin (Embed-812, Electron Microscopy Science) in ethanol. Each infiltration step lasted one hour. The coverslips were inverted on a drop of resin in a plastic mold. Samples were transferred into a vacuum oven at 50 °C to polymerize for 24 h. The coverslips were then removed with repeated immersions of the resin block in liquid nitrogen followed by heat-shocks on a hot plate. Finally, the block was trimmed, and ultrathin sections of 60-70 nm were cut using a diamond knife (Diatome) mounted on an ultramicrotome (Leica UltraCut UCT). Section were placed on 200 mesh pioloform coated index grids and counterstained first with uranyl acetate (Electron Microscopy Science) and lead citrate (Leica). Samples were visualized using a transmission electron microscope (TEM), JEOL JEM-200CX, equipped with an AMT XR-100 CCD camera or a JEOL JEM 1400 equipped with an AMT XR-111 CCD camera.

In some experiments, preceding fixation, cells were stimulated for 90 seconds with a solution containing 70 mM KCl, 10mM Hepes, 10mM glucose, 60 mM NaCl, 1 mM $MgCl_2$ and 2 mM $CaCl_2$. The pH was adjusted to 7.3 with NaOH and osmolarity ~310 mOsm. The quantification of event frequency, from single sections, was done using the software ImageJ (Schindelin, Arganda-Carreras et al. 2012). The number of clathrin curvatures formed at the flat plasma membrane, endosomes and bulk invaginations in 40 cells (cross sections) was counted and divided by the area of each cell **(paper I).** To identify the real number of bulk invaginations, endosomes within 400 nm from the plasma membrane were traced in serial ultrathin sections at TEM to capture possible connections with the plasma membrane. The percentage of bulk invaginations was calculated, and a correction was applied to the frequency plot of the clathrin profiles originating from the bulk invaginations identified at the single section based. For the statistical analysis, significance and P-values were calculated using unpaired Student's t-test (two-tailed).

Cells on coverslips were fixed **(paper I, III, IV)** with a mixture of 2% glutaraldehyde, 2% paraformaldehyde (Electron microscope science) and 4% tannic acid (Sigma) in 0.1 M cacodylate buffer pH 7.3 for 15 min. The same fixative was used without tannic for an additional 15 min. Samples were incubated with a solution 100mM glycine in 0.1 M cacodylate for 5 min and then with just 0.1 M cacocylate buffer three times for 5 min. Subsequently, cells were post-fixed with a solution of 1% $OsO_4$ in 0.1 M Cacodylate for 60 min on ice, then rinsed in 0.1 M cacodylate three times and 1 time in $ddH_2O$, before gradually dehydration increasing solution of pure ethanol in $ddH_2O$ (25%, 50 %, 70 %), two times for each dilution for 5 min. Later, samples were stained with 2% uranyl acetate (Electron Microscope Science) in 70 % ethanol for 30 min followed by dehydration (85%, 95%) till 100% ethanol. Lastly, samples were infiltrated with increasing concentrations

(25%, 50%, 70%, 100%) of epon resin (Embed-812, Electron Microscopy Science) in ethanol. Each infiltration step lasted one hour. The coverslips were inverted on a drop of resin in a plastic mold. Samples were transferred into a vacuum oven at 50 °C to polymerize for 24 h. The coverslips were then removed with repeated immersions of the resin block in liquid nitrogen followed by heat-shocks on a hot plate. Finally, the block was trimmed, and ultrathin sections of 60-70 nm were cut using a diamond knife (Diatome) mounted on an ultramicrotome (Leica UltraCut UCT). Section were placed on 200 mesh pioloform coated index grids and counterstained first with uranyl acetate (Electron Microscopy Science) and lead citrate (Leica). Samples were visualized using a transmission electron microscope (TEM), JEOL JEM-200cx, equipped with an AMT XR-100 CCD camera or a JEOL JEM 1400 equipped with an AMT XR-111 CCD camera.

In some experiments, preceding fixation, cells were stimulated for 90 seconds with a solution of containing 70 mM KCl, 10mM Hepes, 10mM glucose, 60 mM NaCl, 1 mM $MgCl_2$ and 2 mM $CaCl_2$. The pH was adjusted to 7.3 with NaOH and osmolarity ~310 mOsm. The quantification of event frequency, from single sections, was done using the software ImageJ (Schindelin, Arganda-Carreras et al. 2012). The number of clathrin curvatures formed at the flat plasma membrane, endosomes and bulk invaginations in 40 cells (cross sections) was counted and divided by the area of each cell **(paper I).** To identify the real number of bulk invaginations, endosomes within 400 nm from the plasma membrane were traced in serial ultrathin sections at TEM to capture possible connections with the plasma membrane. The percentage of bulk invaginations was calculated, and a correction was applied to the frequency plot of the clathrin profiles originating from the bulk invaginations identified at the single section based. For the statistical analysis, significance and P-values were calculated using unpaired Student's t-test (two-tailed).

### 3.2.6 High pressure freezing and freeze substitution

Primary bovine chromaffin cells were prepared following a modified version of O'Connor et al. 2007 protocol. After digestion the medulla was minced in Lock's buffer and filtered through a 250 µm sterile nylon mesh. The filtrate was centrifuged at 49 g for 4 min (O'Connor, Mahata et al. 2007). The supernatant was then removed, and the pellets resuspended in pre-warmed DMEM low glucose medium supplemented with 10% fetal bovine serum. Lastly, cells were sedimented by gravity and the medium carefully removed. Around 5 µl of cell pellet was transferred to a 3 mm Type-A planchet with a depth of 200 µm pre-coated with DOPC lipids, paying attention to fill all the spaces. After that, a Type-B planchet was placed on top with the flat surface facing down to seal the assembly. The

assembled specimen chamber was frozen using a Leica EM ICE high-pressure freezing system. The frozen samples were transferred to cryovials in liquid nitrogen vapor and transferred to a pre-cooled (-90 °C) freeze substitution unit (Leica EM AFS). No heavy metal stain ($OsO_4$) was needed for the preparation. Freeze substitution was performed using a solution of 1% tannic acid in dry acetone for 24 h followed by an exchange to a mixture of 2% uranyl acetate, 1% glutaraldehyde and 3% H2O in acetone for 21 h. Then the samples were washed 3 times for 1 hr with dry acetone. The temperature was slowly raised from -90 °C to -30 °C in 96 h (0.6 °C/h) and again from -30 °C to 15 °C in 36 h (1.25 °C/h). Samples were separated from the planchets in acetone and infiltration was performed in increasing concentrations of Embed-812. Ultrathin sections (50-60 nm) were cut on a Leica EM UC7 ultramicrotome and poststained with lead citrate for 5 min. Digital micrographs were acquired on a JEOL JEM-200CX operating at 120kV and equipped with a bottom mounted AMT XR-100 CCD camera **(not included in paper III)**.

### 3.2.7 Cell unroofing and platinum replica electron microscopy

Bovine chromaffin cells plated on coverslips were immersed in stabilization buffer containing 70 mM KCl, 30 mM HEPES brought to pH 7.4 with 5 M KOH, 5 mM $MgCl_2$, 3 mM EGTA for 2 min and splashed with a syringe filled with stabilization buffer and 4% paraformaldehyde (2% final concentration). The coverslips were then transferred to 2% glutaraldehyde in stabilization buffer and incubated 20 min at 4°C. Cells were stimulated in some experiments, using a solution containing 70 mM KCl, 10mM Hepes, 10mM Glucose, 60 mM NaCl, 1 mM $MgCl_2$ and 2 mM $CaCl_2$. The pH was adjusted to 7.3 with NaOH and the osmolarity to ~310 mOsm. The stimulation lasted 45 sec followed by rinsing in bath solution for another 45 sec (125 mM NaCl, 10 mM glucose, 10 mM HEPES, 5 mM $CaCl_2$,1 mM MgCl2, 4.5 mM KCl, and 20 mM TEA, pH 7.3 adjusted with NaOH) before the immersion in the stabilization buffer (Fig. 4).

All the samples were then moved to 0.1% tannic acid freshly dissolved in water for 20 min **(paper I)**. They were then rinsed 4x with water and placed in 0.1% uranyl acetate for 20 min. The coverslips were then dehydrated, critical point dried, and coated with platinum and carbon as previously described (Sochacki, Larson et al. 2012). The region of interest on the coverslip was imaged with 10x phase contrast to obtain a map of the imaged region. The replicas were lifted as previously described (Sochacki, Shtengel et al. 2014) and placed onto Formvar/carbon-coated 75-mesh copper TEM grids (Ted Pella 01802-F) that had recently been glow-discharged. Some cells were lost behind grid bars. TEM imaging was performed as previously described at 15,000x magnification (1.2 nmper pixel) using a

JEOL 1400 and Serial EM freeware for montaging (Mastronarde 2005). The density of the clathrin curvatures was calculated using the software ImageJ (Schindelin, Arganda-Carreras et al. 2012) counting the number of clathrin curvatures divided by the cell area. Significances and P-values were calculated using unpaired or Student's t-test (two-tailed) was used for the statistical analysis.

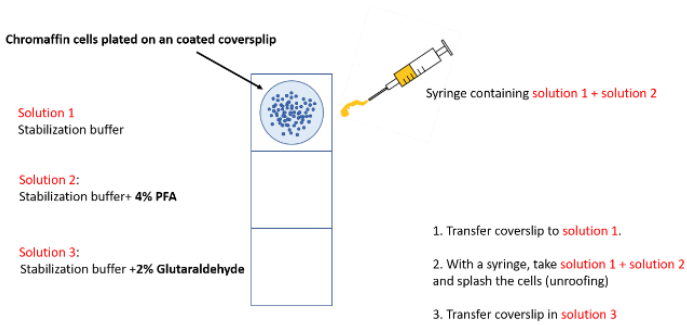


Figure 4 - The scheme describes the unroofing process. Coverslips first immersed in solution 1 (stabilization buffer), then splashed with solution 2 (stabilization buffer + 4% PFA) and transferred to solution 3 (stabilization buffer + 2% glutaraldehyde ).

## 3.3 Giant reticulospinal axon in lamprey

### 3.3.1 Intra-axonal microinjection and electrophysiology

For the study **(paper II)** adult lampreys near the end of their life cycle with a length around 20-30 cm were used. The lampreys were kept in an aquarium at 4 °C. The day of the experiment the animal was anesthetized with MS-222 (tricainemethanesulfonate) and decapitation was made just before the gills. The spinal cord was isolated in a Ringer's solution made of 91mM NaCl, 2.1 mM KCI, 2.6 mM $CaC1_2$, 1.8 mM $MgC1_2$, 4 mM glucose and 2mM HEPES at pH 7.4 previously oxygenated and chilled at 6-8 °C and placed with pin ventral side up on a Sylgard piece placed in a chamber containing the same solution. Under an optical microscope meninges were removed and a pin (~100 µm in diameter) was applied at the site of the injections as reference (Shupliakov, Low et al. 1997). The activity of the spinal cord was recorded by two electrodes place at the rostral/caudal side. Glass pipettes with a resistance of 50-90 MΩ were used to impale the giant axons. The pipette was filled with the proper reagent, a fluorophore (Texas red or Alexa 488 tagged with the protein of interest) and a buffer made (injection buffer) of 250 mM KAc and 10mM HEPES (pH 7.4). Once the axon was identified, a small pressure was applied to the pipette to inject the reagent. The injection was monitored with a CCD camera (charge-coupled device) connected to a fluoresce microscope. The concentration of the reagent injected was indirectly measured considering the decay of the fluorescence along the axon (Fig. 5). The microinjection pipettes contained latrunculin A (60 mM) and Cyto D

(33 mM), and phalloidin-Alexa Flour 488 (1,200 U /µl; Invitrogen) in the injection buffer. Compounds were diluted in Texas red. Texas red was also used alone with the injection buffer for control injections. Giant axons were stimulated using an extracellular electrode placed at the rostral side at 5 Hz for 20-30 min. In the case of control experiments, the stimulation was applied intracellularly by impaling the axon. Action potentials were recorded with an extracellular electrode placed at the caudal side.

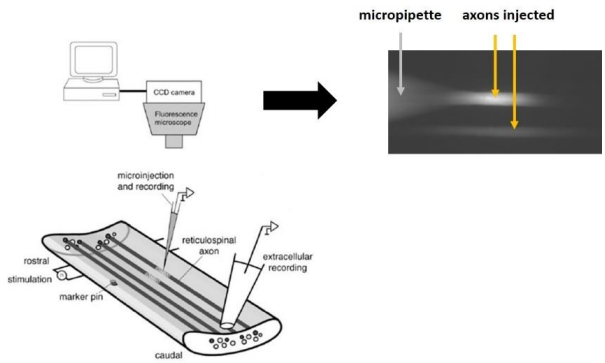


Figure 5 - Schematic drawing showing the intra-axonal microinjection. The spinal cord is facing up and the activity was recorded by two electrodes placed at the rostral and caudal side. The glass electrode was filled with a fluorophore and the injection was monitored with a CCD camera connected to a fluorescence microscope. On the right side a CCD camera picture shows a micropipette and 2 axons injected with Texas red.

### 3.3.2 Confocal imaging

The fluorescence of the microinjection of A488-phalloidin was detected using a Nikon D-eclipse C1 confocal microscope using a 100x objective with NA 1.0. For control experiments we used a 10x air objective and a 40x water immersion objective with 0.8 NA. The data were sampled from two areas along the axon with a distance between each other of ~300-500 nm and analyzed using Student's t-test.

### 3.3.3 Electron microscopy from spinal cord tissue

The spinal cords were fixed during stimulation with a solution made fresh of 4% tannic acid, 3% glutaraldehyde and 0.5 % paraformaldehyde in 0.1 M cacodylate buffer at pH 7.4 for 1 h at 4 °C followed by the same solution without tannic acid for 3 h at 4 °C. Glutaraldehyde reacts with free amines and produces fast (within few minutes) irreversible cross-linking networks through the cytoplasm, paraformaldehyde cross-links free amino groups of proteins and nucleic acids (slower than glutaraldehyde) and tannic acid enhances the contrast of proteins (Eltoum, Fredenburgh et al. 2001). The reaction of the cocktail drops the pH considerably, so the use of an adequate buffer like cacodylate is important. Used together, these reagents create a nice contrast essential for the visualization of membranes. The solution was washed 3 x 10 min with 0.1 M cacodylate buffer and post-fixed with 1% osmium tetroxide ($OsO_4$) in $ddH_2O$ for 1 at 4 °C. Osmium tetroxide reacts

with unsaturated bonds of lipids and phospholipids. During post fixation osmium tetroxide is reduced to lower oxides that are deposited in the tissue, particularly on membranes, showing the characteristic black heavy stain. The specimen was then rinsed in dd$H_2O$ and the water contained in the samples was removed (dehydration) by adding increasing concentrations of ethanol to 70%, where 2% uranyl acetate in 70% ethanol was added for 1 h at 4 °C. The samples were washed with 70% ethanol and dehydration continued with increments of ethanol to 100%. Lastly, the spinal cord was embedded in Durcapan ACM (Fluka) and serial ultrathin sections of 60-70 nm were cut using a diamond knive (Diatome) and an ultramicrotome (Leica UltraCut UCT). Sections were placed on single slot grids precoated with formvar. The grids were visualized with a Tecnai 12 electron microscope (FEI). The sections were made at distances larger than 100 µm from the injection site. The analysis was done on 5 synapses cut in serial sections. Significances and P-values were calculated using one-way analysis of variance (ANOVA) followed by the multiple pairwise comparisons using Holm–Sˇıˊdaˊk method (GraphPad Prism 6).

# 4 RESULTS AND DISCUSSION

## 4.1 To determine whether bulk membrane invagination serves as a platform for clathrin-dependent endocytosis to take place (paper I)

With conventional electron microscopy, platinum replica electron microscopy and super-resolution stimulated emission depletion (STED) microscopy on live chromaffin cells we investigated the role of bulk invaginations as a possible precursor of clathrin-mediated endocytosis.

### 4.1.1 Observing clathrin-coated pits at the flat plasma membrane, bulk plasma membrane invaginations and endosomes

We examined clathrin-coated pits with conventional EM in bovine adrenal chromaffin cells in primary culture in resting conditions and in the presence of 70 mM KCl that triggered exocytosis and subsequent endocytosis by depolarization. Cells were fixed, embedded and sectioned before EM examination. At single sections across chromaffin cells (**Paper I**, Fig. 1a), we observed clathrin-coated pits or clathrin-coated membrane patches at the flat plasma membrane (**Paper I**, Fig. 1b), at large Ω-shape membrane invaginations at the plasma membrane (Fig. 6), and at endosome-like structures in the cytosol that were not apparently connected to the plasma membrane (**Paper I** , Fig. 1d).

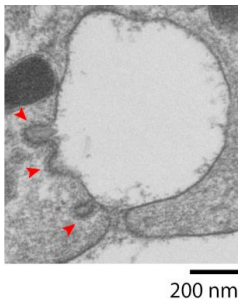


Figure 6 – EM micrographs of a bulk invagination connected to the plasma membrane with clathrin-coated curvatures budding off (arrows).

In some experiments, we performed serial ultrathin sections, which allowed us to resolve clathrin-coated patches in the whole volume of the structure, including the entire bulk invagination (**Paper I**, Fig. S1e). Such serial sections allowed us to identify bulk membrane invaginations that appeared as endosome-like structures in the cytosol in one section, but were actually connected to the plasma membrane. The presence of clathrin-coated pits at the bulk invaginations, flat plasma membrane and endosome-like structures suggests that clathrin-coated vesicles are generated from these three different structures (**Paper I**, Fig. 1e). In resting conditions, more clathrin patches were observed at the flat plasma membrane than at the bulk invaginations per unit area of the cell cross section (Fig. 7 a-b, white bar). In the presence of 70 mM KCl, clathrin-coated patches were not increased significantly at the flat plasma membrane (Fig. 7a, grey bar), but significantly increased at bulk invaginations (Fig. 7b, grey bar), suggesting that clathrin-mediated endocytosis take places primarily from the bulk invaginations after KCl-induced depolarization.

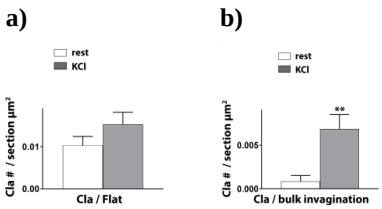


Figure 7 - Bar graph showing clathrin patch frequency at the flat plasma membrane (a) and bulk invaginations (b) per unit ($\mu m^2$) area of the cell cross section in resting condition and in the presence of 70 mM KCl (n=40 cell cross-sections from both conditions, mean =s.e.m.; *<0.05; **<0.01, ***<0.001, student-t-test).

In the above experiments, the number of bulk invaginations were identified in single sections. Such a criterion may lead to underestimation of the number of bulk invaginations, because a single section may miss the pore region. Indeed, in a set of experiments where serial ultrathin sections were made, we found that 58% of endosome-like structures (7 out of 12 structures) within 400 nm from the plasma membrane were actually connected to the plasma membrane (**Paper I**, Fig. S1e), and thus should be re-classified as bulk invaginations. Accordingly, the number of bulk invaginations in Fig. 7b was underestimated. Based on the serial sections, we provided a corrected bar graph showing an even larger contribution of clathrin-coated patches at the bulk invaginations (**Paper I**, Fig.

S1f-g), further confirming bulk invagination as the main site for the generation of clathrin-coated pits at the plasma membrane.

### 4.1.2 Clathrin-coated pits observed at bulk invaginations revealed using platinum replica EM on unroofed chromaffin cells

Platinum replica electron microscopy on unroofed cells allows to reveal unequivocal clathrin-coated plaques or pits right at the plasma membrane (Hirokawa and Heuser 1981, Collins, Warrington et al. 2011, Sochacki, Dickey et al. 2017). We used this technique to verify and strengthen our results obtained with conventional EM. Bovine chromaffin cell were unroofed after 45 sec of 70 mM KCl application. In unroofed chromaffin cells (**Paper I**, Fig. 2a), we observed clathrin-coated pits at the flat membrane (**Paper I**, Fig. 2b) and at a fraction of the large invaginations at the plasma membrane (Fig. 8). We also observed large dense-core vesicles attached to the plasma membrane (**Paper I**, Fig. 2d). Endosome-like structures were not observed because unroofing washed out structures not connected to the plasma membrane. Similar to the conventional EM data, application of 70 mM KCl significantly increased the clathrin-coated pit number at the bulk invagination (**Paper I**, Fig. 2f), but not at the flat membrane (**Paper I**, Fig. 2e). These results consolidate our finding that the primary site for clathrin-coated pit generation at the plasma membrane is not the flat membrane, but the bulk invaginations induced after KCl-induced exocytosis.

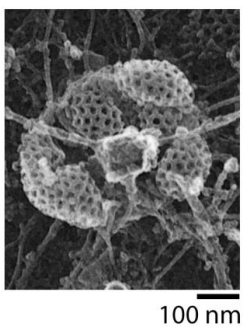


Figure 8 – EM micrograph from an unroofed chromaffin cell shows a bulk invagination covered by clathrin patches.

### 4.1.3 Clathrin labelling in live cells

To determine whether the localization of clathrin-coated pits and patches observed in fixed cells can be observed in live cells, we overexpressed clathrin light chain attached with mTurquoise (clathrin-mTurquoise) to label clathrin, and we overexpressed mNeonGreen attached to phospholipase C delta PH domain ($PH_G$) which binds to PtdIns(4,5)P2 ($PIP_2$) located at the plasma membrane and thus labels the plasma membrane (Lomasney, Cheng et al. 1996, Zhao, Hamid et al. 2016). Confocal imaging shows that the majority of clathrin puncta were localized near the plasma membrane at the cell bottom, but not at the cell

center (**Paper I**, Fig. 3a). Super-resolution STED microscopy at the microscopic XZ plane revealed clathrin spots at the flat plasma membrane (**Paper I**, Fig. 3b, d) and at bulk membrane invaginations (Fig. 9a). At a given XZ plane, we did not observe clathrin spots in every bulk invagination (4 out of 30 bulk invaginations at a given XZ plane were associated with clathrin spots). This is likely because clathrin spots were out of the imaged XZ focal plane. Consistent with this possibility, 3-dimensional reconstruction of some $PH_G$ -labelled bulk invaginations showed association of multiple clathrin spots (Fig. 9b), suggesting that clathrin is also clustered at bulk invagination in live cells. We did not examine endosome-like structures, because $PH_G$ only labelled the plasma membrane. Interestingly, STED imaging of $PH_G$ -labelled membrane at the XZ plane every 26-300 ms revealed that after depolarization (-80 to +10 mV, depol1 s) $PH_G$ -labelled vesicles were pinched off from bulk invaginations (**Paper I**, Fig. 3f, n = 5 events). These results provide live-cell evidence showing that membrane budding indeed can occur from bulk invagination of Ω-shape profiles at the plasma membrane.

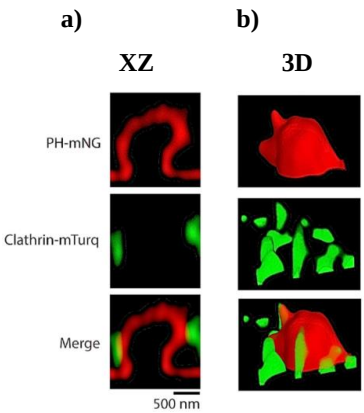


Figure 9 - a) XY STED images of a bulk invagination of the plasma membrane that colocalize with Clathrin-mTurq. b) 3D reconstruction of a XYZ stack showing a bulk invagination surrounded by clathrin spots. Top, $PH_G$; middle, Clathrin-mTurq; bottom, merge.

### 4.1.4 Discussion

With conventional EM, platinum replica EM and super-resolution STED live cell imaging in the neuroendocrine chromaffin cells, we observed clathrin-coated pits at the flat plasma membrane, large bulk membrane invaginations at the plasma membrane, and in cytosolic endosome-like structures. Surprisingly, depolarization-induced exocytosis was followed by an increase of clathrin-coated pits at the bulk membrane invaginations, but not at the flat plasma membrane, suggesting that bulk membrane invaginations are the site for exocytosis-induced clathrin-mediated endocytosis at the plasma membrane. In live cells, we observed clathrin spots at the flat plasma membrane and bulk invaginations at the plasma membrane;

we also observed PHG-labelled vesicles pinching off from bulk membrane invaginations. These results provide the first live-cell evidence indicating the existence of vesicle pinch-off from bulk membrane invaginations after depolarization. These results suggest that bulk membrane invaginations at the plasma membrane are the primary sites for clathrin-mediated endocytosis taking place in secretory cells.

## 4.2 To determine whether F-actin is involved in providing force to mediate post-fusion structural changes and the merging of vesicles with the plasma membrane (paper II)

To investigate the role of actin in vesicle fusion, live bovine chromaffin cells were visualized in a confocal microscope and fixed lamprey reticulospinal spinal axons screened with an electron microscope. Both models were treated with actin perturbing agents: Cytochalasin D (Cyto D) and Latrunculin A (Lat A). Cyto D is fungal metabolite that binds actin filaments and block polymerization. Cyto D  bind to the barbed end of actin filaments, then blocking both the assembly and disassembly of individual actin monomers from the bound end (Cooper 1987) (Fig. 10a).

Lat A is a natural toxin purified from the red sea sponge Latrunculia magnifica. It was initially found to inhibit actin polymerization and disrupt the arrangement of F-actin. It sequesters actin monomers, preventing actin polymerization, thereby promoting filament disassembly (Spector, Shochet et al. 1989) (Fig. 10b).

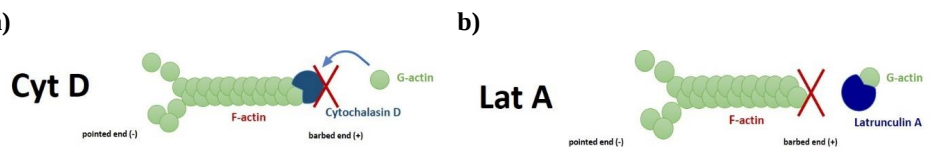


Figure 10 - Actin perturbation agents' mechanism. a) Cyto D acts as a cap protein at the barbed end of the filament and prevents further polymerization; b) Lat A sequesters actin monomers preventing polymerization and promoting disassembly.

### 4.2.1 F-actin dynamics mediates Ω-profile merging in live chromaffin cells

With a new technique recently developed (Chiang, Shin et al. 2014), it has been possible to visualize the Ω-profile merging into the plasma membrane. The Ω-profile merging could change in three patterns: 1) the Ω-profile shrinks until undetectable (termed Ω-shrink), 2) the Ω-profile stays maintaining its size (termed stay fusion) and 3) the Ω-stay fusion is

followed by pore closure (termed close fusion) (Fig. 11a). To induce fusion events, the cells were whole-cell voltage-clamped and depolarized with 10 pulses of 50 ms at 2Hz., 69 % were Ω-shrink, 29% stay fusion and 3% pore closure (From 192 events in 18 cells, Fig. 11b).

**a)** **b)**


Figure 11 - Three categories of Ω-profile merging into the PM. a) Schematic diagram showing the exo-endocytosis model. The profile may stay at the site (stay fusion), close the pore (close fusion) or shrink until undetectable (Ω-shrink). b) Percentages of Ω-shrink, stay and close fusion upon depolarization induced by $Train_{2Hz}$.

Cells were treated with Lat A or Cyto D to block actin dynamics. In the preparations, the equilibrium of Ω-profiles shifted from Ω-shrink to stay fusion. The block of actin slows down the Ω-shrink profiles that are converted into stay fusion. No change was detected in close fusion (Fig. 12). Additionally, since actin dynamics requires ATP for the elongation of the filaments (Dayel, Holleran et al. 2001, Sablin, Dawson et al. 2002) we added the non-hydrolyzable analogue ATPγS into the bath solution to mimic the action of the actin blockers. Similar to the cells treated with Cyto D and Lat A, we observed an increase of stay fusion events and a reduction of Ω-shrink events. These results suggest that the dynamics of actin is needed to merge the Ω-profile with the plasma membrane in live chromaffin cells.

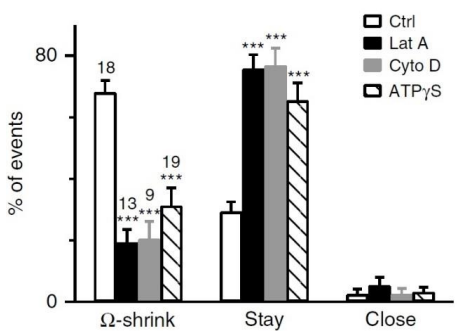


Figure 12 - Actin perturbation inhibits Ω-shrink but promotes stay fusion. Percentages of Ω-shrink, stay and close fusion upon depolarization induced by $Train_{2Hz}$ in control, Lat A, Cyto D and ATPγS. Cell numbers are shown on top of the bars.

### 4.2.2 Actin perturbation causes accumulation of Ω-profiles at the active zone in synapses

To determine whether actin mediates Ω-profile merging at synapses, we microinjected a mixture of Lat A/Cyto D (60 µM/33 µM) in the reticulospinal axon in lamprey and screened the giant synapses by EM. The reason why we used a concentration ~10 times higher in the micropipette is because, following microinjections, the solution was diluted in the studied regions (Fig. 13).

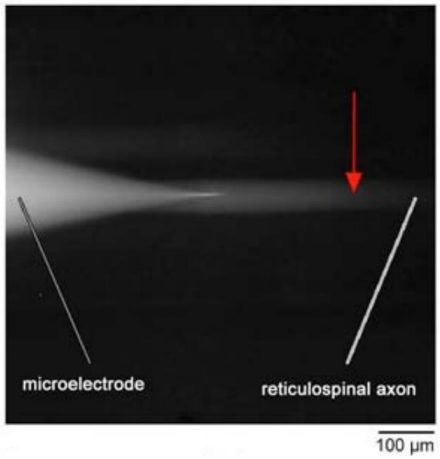


Figure 13 - CCD camera image shows a reticulospinal axon injected with Lat A/Cyto D and Texas Red. Texas red is used to monitor the microinjection. The red arrow represents the region of study. We estimated a reduction of fluorescence of ~10 folds in this region.

Upon injections, no significant difference in synaptic vesicle number was noticed compared to control (**Paper II**, S12b-e) and the propagation of the action potential along the axon was normal (**Paper II**, S12f) proving that the injections neither affected active zone morphology nor action potential propagation. Following injections synapses were stimulated with action potentials at 5Hz for 20 - 30 min and fixed for EM screening (Shupliakov, Bloom et al. 2002). The giant synapse was examined in serial sections and Ω-profiles structures defined with a pore equal or smaller than their width (Fig. 14).

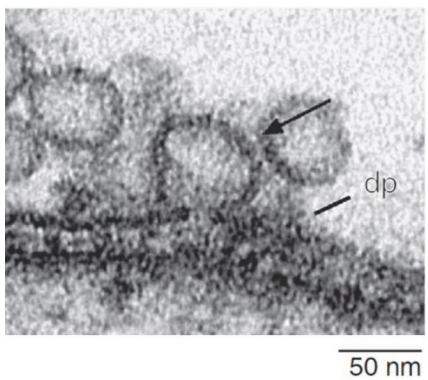


Figure 14 - EM micrograph of a Ω-profile merging to the plasma membrane. The Ω-profile is marked with an arrow. dp, dense projection of the active zone.

The analysis of five synapses in serial section from three axons, showed a significant increase of Ω-profiles in LatA/Cyto D-injected preparations compared to control (Fig 15).

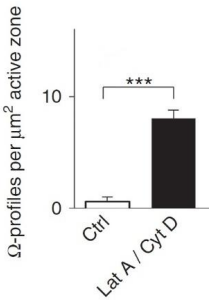


Figure 15 - Quantification of Ω-profiles accumulated at the active zone. The number of Ω-profiles per $\mu m^2$ at active zones in control (Ctrl) axons and in axons microinjected with Lat A/Cyto D.

The above results are consistent with those obtained in live chromaffin cell and suggest that F-actin promotes Ω-profile merging into the PM. Two sets of experiments further support this suggestion. First, we labelled the giant synapse with a monoclonal actin antibody for post-embedding immune EM (Bloom, Evergren et al. 2003) to see whether actin was localized at the active zone. The number of gold particles was higher near the plasma membrane (within 100 nm, Fig. 16) of the active zone than the reserve pool (> 200 nm from the PM of the active zone).

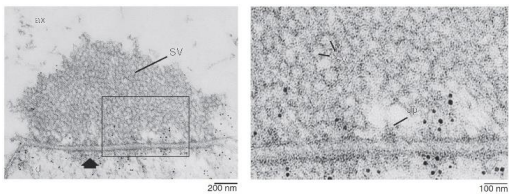


Figure 16 - Actin labeling by Immunogold EM. The Micrograph on the left shows gold particles that bind actin in a giant synapse with synaptic vesicle pool (SV), active zone (thick arrow), axon (ax) and dendrite (d). On the right, a high mag of the box from the left image.

It was also significantly higher than outside the active zone (> 300 nm far away from the active zone, Fig. 17a-b) indicating that the actin network is denser near the active zone where fusion occurs (Fig. 17a-b).

**a)** **b)**

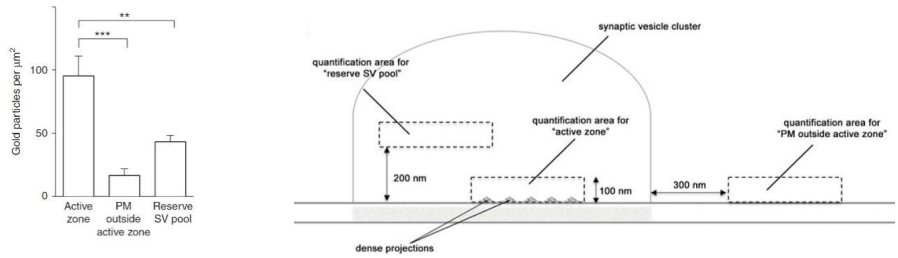


Figure 17 - ImmunoEM quantification. a) The bar graph shows the number of gold particles localized at the active zone, reserve pool and outside the active zone. b) The scheme shows the three areas of quantification

An additional evidence that confirms the high density of actin at the active zone was given using F-actin labelled with phallodin-Alexa 488. Phalloidin is a toxin found in the death cap mushroom of the *Amanita phalloides.* It binds to actin filaments at a ratio of one molecule for one or two actin protomers and lock adjacent actin subunits together. In this way, depolymerization is not possible and the equilibrium is shifted to assembly. Blocking depolymerization drastically reduces the concentration of free actin monomers, leading to a reduction of actin dynamics (Cooper 1987). Following microinjection of phalloidin- Alexa 488 fluorescence accumulated in spots in the axon (Fig. 18), consistent with previous work (Evergren, Gad et al. 2007) in which each spot corresponded to an active zone and its surrounding periactive zone.

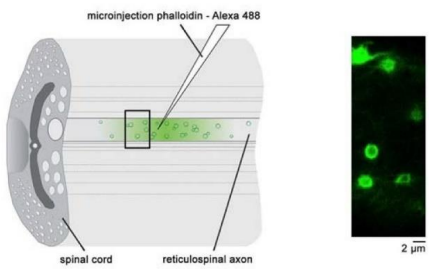


Figure 18 - Microinjection of phalloidin - Alexa 488 labels F-actin. The schematic on a) shows the injection of a reticulospinal axon. The box marks an area that was screened by confocal microscopy. In b) a confocal picture showing actin labeling at the synapse.

Lastly, to confirm the action of LatA/Cyto D in disrupting actin filaments, we set up a control experiment. One axon was injected with Lat A/Cyto D and Texas red first, then with phalloidin Alexa 488 15 min later ~800 nm away from the first injection. Then, we measured the fluorescence of phalloidin Alexa 488 ~300-500 nm away from the Lat A/Cyto D injection and we detected a reduction of phalloidin puncta compared to the axon injected with Texas red only (**paper II**, S14 b-d). Taken together these results suggest that F-actin is involved in mediating Ω-profile merging at the neuronal nerve terminal.

### 4.2.3 Discussion

The above data showed that actin dynamics is needed to merge the Ω-profile to the plasma membrane. This finding can presumably be applied to many other models containing large dense core vesicles such as β-cells that release insulin, glia cells, cell bodies of neurons and nerve terminals that secrete dopamine or neuropeptides crucial for brain functions (Wu, Hamid et al. 2014). These findings might also be applicable to small synaptic vesicles (~30-50 nm) because actin perturbation caused accumulation of Ω-profiles at the active zone of giant synapses in lamprey. The synaptic endo-exocytic cycle has been suggested to resemble that of chromaffin cells (Lindau and Alvarez de Toledo 2003, Alabi and Tsien 2013). Unfortunately, at the moment we are not able to visualize synaptic vesicle fusion in live cells given the diffraction limits. Several studies suggest an involvement of actin in the fusion process, for example in a model containing vesicles of 1-5 µm (*Xenopus oocytes* (Sokac, Co et al. 2003), lacrimal epithelial acinar cells (Nightingale, White et al. 2011), and pancreatic acinar cells (Nemoto, Kojima et al. 2004) in which vesicle fusion is followed by an F-actin coating that might squeeze the Ω-profile to release its content. It was also suggested that in chromaffin cells F-actin squeezes large-dense core vesicles undergoing fusion. Our results suggest that the force needed to release the vesicular content might come primarily from the membrane tension provided by F-actin.

Ω-profile merging has been assumed to be a passive event with no energy consumption once the vesicle fusion has been initiated. Our results suggest that this view is incorrect since actin polymerization needs ATP hydrolysis to merge the Ω-profile to the plasma membrane. We conclude that the consumption of ATP for Ω-profile merging is a factor to take in consideration in diseases that affect F-actin dynamics (e.g., periventricular heterotopia) (Lian and Sheen 2015), and in the mitochondrial dysfunctions that have been implied in Alzheimer's disease, Parkinson's disease and Huntington's disease (Hroudova, Singh et al. 2014).

## 4.3 To determine whether F-actin is involved in providing force to regulate structural changes of dynamic fusion pores (paper III)

Chromaffin cells were transfected with mNeonGreen tagged with phospholipase C delta PH domain and bathed with Atto 532 (a membrane impermeable dye). PH-mNeonGreen binds PIP2 labelling the plasma membrane at the cytosolic side. The cell was depolarized, and capacitance changes recorded. Atto 532 diffused from the bath to Ω-profiles generated by fusion (labelled with PH-mNEONGreen, **paper III**, Fig. 3). The different structural

changes of the pore (opening, expansion, constriction and closure) were visualized, reflecting fusion and fission efficiency.

To further confirm the existence of fusion pores of the Ω-profiles we performed electron microscopy experiments. First, chromaffin cells were stimulated with KCl, fixed and screened by TEM. Micrographs showed Ω-profiles with pore sizes between 12-430 nm. All Ω-profiles did not contain a dense core (n = 53) (**Paper II**, Fig. 2), suggesting that the dense core can be released via a pore narrower than the dense core. Second, to confirm that the fusion pore sizes were not due to distortions induced by aldehyde fixatives and EM processing, cells were rapidly frozen by a high-pressure freezing (HPF) device and freeze-substituted (unpublished data). This approach preserves cell structure and morphology close to the native state[1]. The pore sizes of the Ω-profiles observed followed the trend observed in both live cells and chemically fixed preparations (Fig. 19)

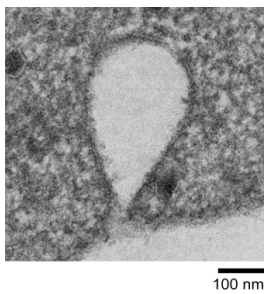


Figure 19 - EM micrograph of a Ω-profile captured by high pressure freezing and freeze substitution. The pore has a diameter of ~30 nm.

The results from **Paper II** (Wen, Grenklo et al. 2016) suggested that the application of latrunculin A to chromaffin cells depolymerized F-actin and reduced membrane tension that consequently inhibited shrink-fusion. To test whether F-actin is also involved in structural changes of the pore, we applied the same actin-directed compound to the bath. Latrunculin A reduced the percentage of $Pore_v$ (an Ω-profile with a pore bigger than the STED resolution of ~60 nm), suggesting that F-actin-dependent membrane tension is needed for pore expansion.

[1] Gianvito Arpino, Ling-Gang Wu, Christopher Bleck. Ultrastructural Preservation and Improved Visualization of Membranes in Primary Bovine Chromaffin Cells. October 2019. Leica-Microsystem. https://www.leica-microsystems.com/science-lab/ultrastructural-preservation-and-improved-visualization-of-membranes-in-primary-bovine-chromaffin-cells/

### 4.3.1 Discussion

The fusion pore theory suggests the existence of a metastable narrow pore (<5 nm) that either closes or expands until the vesicle merges with the plasma membrane (Alabi and Tsien 2013, Wu, Hamid et al. 2014). We found that the metastable pore size ranges from 0 to 490 nm. This large dynamic range of pores that can expand, constrict and/or close is likely to underlie a diversity of rates of content release and vesicle retrieval. Our results suggest that the pore dynamics depends on competition between F-actin/tension-dependent pore expansion and calcium/dynamin-dependent pore constriction (**Paper III**, Fig. 4). These findings will help to study pore dynamics of many biological processes including exocytosis, endocytosis, intracellular trafficking, fertilization, and viral entry.

## 4.4 To identify fusion modes with specific structural changes that control vesicular content release (paper IV)

To correlate fusion modes with structural changes of vesicles and content release, we performed experiments in primary bovine chromaffin cells with a combination of microscopy techniques, including super-resolution STED microscopy, confocal microscopy and EM.

### 4.4.1 Observation of shrinking and enlargement of fusing vesicles

Ω-profile shrinking was observed using a recently developed technique to visualize the hemi-fusion intermediate (Zhao, Hamid et al. 2016). The technique consisted of labelling the PM by transfecting cells with phospholipase C delta PH domain ($PH_G$) attached to EGFP and adding Atto 532 to the bath. The dye entered the fusion Ω-profile to label the fusing vesicle confirming the structural changes. The xzt scan with the STED allowed direct visualization of the vesicle that was undergoing fusion. To induce exocytosis the cell was patch clamped using the whole-cell configuration and depolarized for 1s (**paper IV**, Fig. 1a). Following PH-Ω appearance, the Ω-profile could (236 events, 202 cells) either 1) shrink while maintaining its Ω-shape until it disappeared at the PM (shrink-fusion, Fig. 20 a), 2) shrink partially, then maintaining a reduced-size Ω-profile (partial-shrink-fusion), 3) maintain its Ω-profile (same-size-fusion), or 4) increase in size while maintaining its Ω-shape (enlarge-fusion, Fig. 20b) (**paper IV**, Fig. 1b-h). During shrinking most of the profiles maintained their Ω-shape and decrease their width and height proportionally. However, in other examples the shrink-fusion was reflected as Ω-profiles with a tubular shape with a height bigger than the width (**paper IV**, Fig 1d-f).

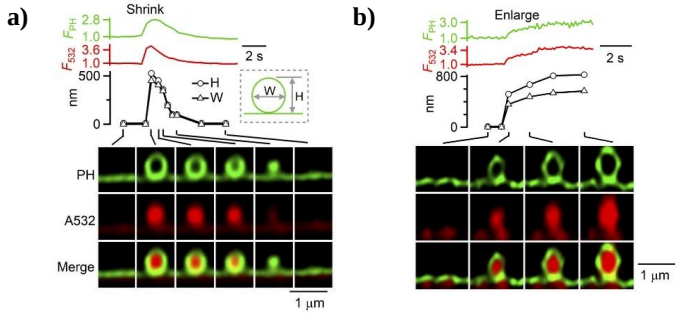


Figure 20 - a) Example of a Ω-profile that shrank while maintaining its shape until fusion with the PM; b) A Ω-profile that increased in size while maintaining its Ω-shape (enlarge-fusion). PH-Ω fluorescence ($F_{PH}$, normalized to baseline), A532 spot fluorescence (F532, normalized to baseline), PH-Ω height (H, circles), PH-Ω width (W, triangles), and sampled images at times indicated with lines showing fusion with various patterns of Ω-profile structural changes.

To confirm the existence of Ω-profile shrinking, we employed EM to visualize the ultrastructure of fusing vesicles. To induce exocytosis, cells were stimulated with a solution containing 90 mM KCl before fixation. Consistent with the results observed in live cells, electron microscopy revealed Ω-profiles with different sizes with width and height correlated (Fig. 21a, c-upper). Moreover, the height/width ratio was mostly > 1 indicating that that Ω-profiles were mostly elongated with some profiles approaching a tubular-shape, consistent with STED observations of mostly elongated Ω-profiles (Fig. 21b, c-lower).

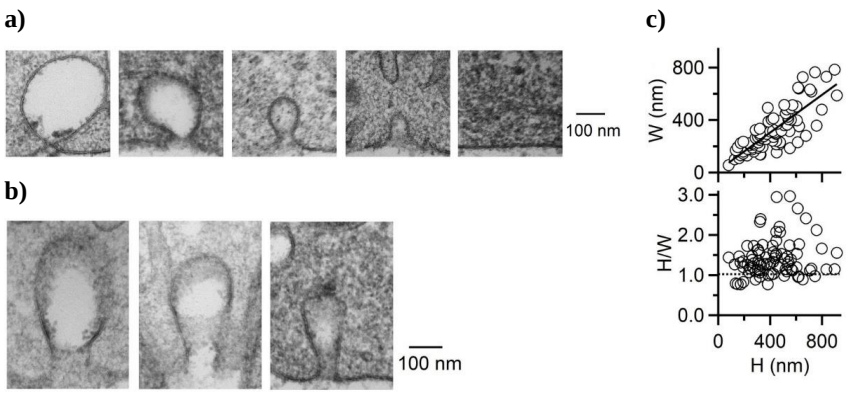


Figure 21 - Ultrastructure of Ω-profiles in KCl stimulated chromaffin cells. a) Micrographs of Ω-profiles with different sizes; b) micrographs of tubular Ω-profiles; c) the upper dot plot shows the ratio between width (W, nm) and height (H, nm). The line is the linear regression fit (correlation coefficient: 0.81). The lower dot plot shows the ratio between H/W and H. Most of the data points are above the dotted line reflecting elongated profiles.

We also examined the pore dynamics corresponding to the four patterns. A visible pore is defined as a pore that exceeded our STED resolution of ~60 nm. The percentage of visible

pores from shrink-related fusion events (shrink$_{related}$-fusion) that include shrink-fusion and partial-shrink-fusion was higher compared to enlarge-fusion, suggesting that enlarge-fusion might employ a smaller pore to release it content (Fig. 22).

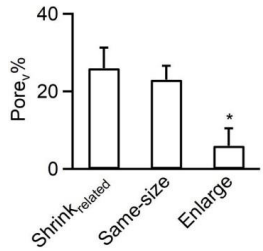


Figure 22 - The percentage of observed Pore$_v$ (Porev%) during shrink-related-fusion fusion (including shrink-fusion and partial-shrink-fusion), same-size fusion and enlarge-fusion (total fusion event number: 236; from 202 cells). *: $p < 0.05$.

### 4.4.2 Measuring content release during shrink-fusion and enlarge-fusion

To determine whether shrink-fusion and enlarge-fusion cause content release with different kinetics, we overexpressed in the cells the vesicular lumen protein neuropeptide Y-EGFP (NPY-EGFP). By confocal microscopy we observed NPY-EGFP and Alexa 647 added to the bath. Upon stimulation vesicle fusion was reflected as a decrease of NPY-EGFP fluorescence and an increase of Alexa 647 (Alexa dye diffuses into the fusing vesicle as soon as the pore opens).

We observed four different patterns: shrink-fusion, partial shrink, same-size fusion and enlarge-fusion (Chiang, Shin et al. 2014)(**paper III**, Fig. 3b-g). By measuring $T_{NPY\_decay}$ we found that shrink$_{related}$-fusion is associated with a much faster release compared to same-size and enlarge-fusion (Fig. 23a). Additionally, $T_{647\_rise}$ was higher in enlarge-fusion compared to same-size and shrink$_{related}$-fusion (Fig. 23b). These results suggest that shrink$_{related}$-fusion might employ a larger pore to release its content than enlarge-fusion.

**a)** **b)**

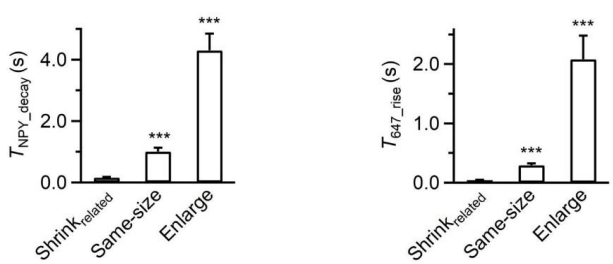


Figure 23 - a) $T_{NPY\_decay}$ (20- 80% $F_{NPY}$ decay time) and b) $T_{647\_rise}$ (20-80% $F_{647}$ rise time) for shrink$_{related}$-fusion (69 events, 28 cells), same-size-fusion (136 events, 28 cells) and enlarge-fusion (31 events, 28 cells).

### 4.4.3 Discussion

The data above suggested that shrink-fusion (or $shrink_{related}$-fusion) is associated with a large fusion pore that facilitates release of vesicle content, while enlarge fusion limits content release by employing a smaller pore. These results challenge the classical view in which kiss-and-run limits release and full-collapse facilitates release. We suggest shrink- and enlarge-fusion as the new yin and yang fusion modes to control content release.

# 5 CONCLUSIONS

This thesis provides insights into membrane-linked mechanisms acting during exo- and endocytosis in excitable cells.

I. Bulk membrane invagination is the primary site for clathrin-mediated endocytosis at the plasma membrane following depolarization-induced exocytosis in secretory cells. A bulk invagination may provide the curvature needed to recruit proteins involved in clathrin-mediated endocytosis and to initiate clathrin-mediated endocytosis (Fig. 24a).

II. F-actin provides sufficient membrane tension to facilitate shrinking of fusion-generated Ω-profiles and may thus merge the fusing vesicle with the plasma membrane in chromaffin cells. F-actin also facilitates Ω-profile merging at lamprey giant synapses, suggesting that F-actin may provide forces for vesicle merging in many types of secretory cells (Fig. 24b).

III. The fusion pore size ranges from 0 to 490 nm in chromaffin cells and yet it is stable. The fusion pore can expand, constrict and/or close at different rates regulating content release. F-actin provides plasma membrane tension to expand the pore and facilitate release. These findings are different from a general belief that fusion either occurs with a maintained narrow pore (< ~5 nm) that subsequently closes or dilates until flattening (Fig. 24c).

IV. Shrink-fusion and enlarge-fusion play opposing roles in the release of exocytotic contents. Shrink-fusion is associated with a larger pore that facilitates content release, whereas enlarge-fusion is associated with a narrower pore that slows down content release. The results challenge the classical view that full-collapse and kiss-and-run serve as the yin and yang fusion modes accounting for rapid/complete and slow/partial release observed in endocrine cells and neurons (Fig. 24d).

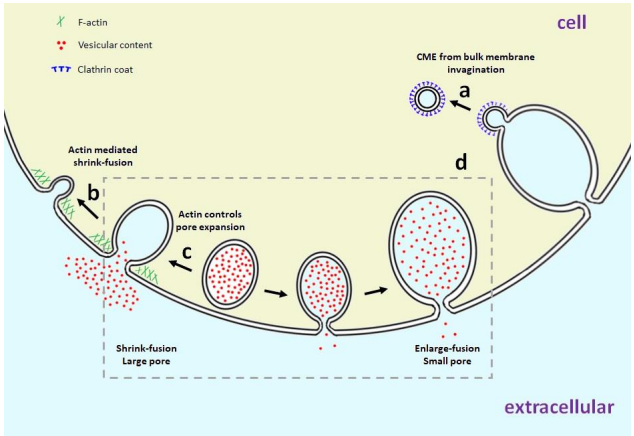


Figure - 24. The model summarizes recent insights into membrane mechanisms during exo- and endocytosis in excitable cells. a) Bulk membrane invaginations are the primary sites for clathrin-mediated endocytosis. b) F-actin provides membrane tension to shrink the fusion-generated Ω-profile and thus merge the fusing vesicle with the plasma membrane. c) F-actin provides plasma membrane tension to expand the pore and facilitate release. d) In the gray dashed box, shrink-fusion is associated with a larger pore that facilitates content release, whereas enlarge-fusion is associated with a narrower pore that slows down content release.

# 6 ACKNOWLEDGEMENTS

I don't believe that this moment has arrived. It was quite an adventure, many obstacles to overcome, even a Covid-19 pandemic threw a monkey wrench into it, but here we are. I recommend this experience to everyone. I would like to thank many people who support me during this path, and I apologize in advance If I forget anyone.

First, I would like to thank my family.
*Mi avete sempre supportato e sopportato. Non vi siete mai lamentati dei miei numerosi spostamenti o dei miei viaggi pazzerelli. Sono davvero contento che siate riusciti a venire sia a Stoccolma che a DC. E' stato bello condividere con voi la mie realta'. Grazie a te nipotino, Gabriel. Spero che diventerai un po' pazzerello come il tuo zio, e girerai un po' il mondo. Grazie a voi.*

I would like to thank my principle supervisor Oleg. I won't be the scientist I am now If wasn't for you. You taught me everything about microscope and how to have a critical scientific thinking. We had some bad moments but who does not have it? I hope we will continue collaborating in the near future. I would like to thank Ling-Gang for accepting me in his lab and gave me the right training and independence. Thanks to my US colleagues Wonchul, Liaho, Chen, Seth. Thanks to Chris, for the best brainstorming sober sessions. I thank Lennart, for being always available and calm in every occasion. To my colleagues in the CMB corridor, Milind, Shaohua, Asa, Olga and Elena. We had some good times. Thanks to Tuomas, for the deep scientific tips.
Thanks to Chiara, who's always been there in the good and bad moments, Fabio, who's still thinks that I am studying biotechnology (bastaaaaaa), Stefano for being my surfer buddy and Jonny. The Piti group for sharing desperation moments, the bbqs, the rave, the latino parties. I can write a lot about that. Anastasia, to show me the Greek tradition of breaking plates. To Argos, the best dog I've ever met, I bet you're running and smelling some doggina ass somewhere in paradise, Sara Opp, thanks for the list, but I am still working on it. Christian to clog my whatsapp chat, Laura to stay with Christian and create the biutiful Bruno, Shaoul, the most social person I 've ever met. Sandraaaaaa, for all the rave party we didn't go, Rapolas for his Russian heritage, Aga, for Jagargatan and Pax. You didn't change. You'll be great neuroscientist or a Shaman one day, Theodora, Jose for your hipster shirts, Jonny for your deep opinions, Simi to bringing me to the longboard world and listen to all my complains, Aida for the cachopo and the out of period Christmas

dinners, Prad Deep for your colorful outfit. Thanks to Ale for the thesis tips, our sushi dinners and holidays meetings between Alezio e Santu Vitu, Mirko, the best flatmate, I'll miss our dying sessions on the couch and Sunday's pizza. Thanks to Paola, Stockholm wouldn't have been a good memory without you. This is was just for the people who shared the first part of my adventure in Stockholm. I would need to write another page for the US, but I don't think anyone will ever read this thesis. Ok, just a couple of sentences. Thanks to Andrea, best pickle ever, and puppy Kaya. To the Tiramisu team, I wouldn't have survived this experience without you, Mimi, the fireplace gossip, briskini and the countless projects, Luiz, picaña, and the squeesh, Burning Man, Stahl, Evelina, chuño, Armando, Mintwood haus, IPA, Anas and its connections, Paula and Ricardo, WSC, Enriquelini and the machismo. To John Lee the omnipresent, Grace for her stylish haircut, Killy and Rita for their New York company and Mr. George, to be the fanciest dog. To parti-Steph, Flash and Roam, Enrica and Pota, Alberto, for the complains, fresh pasta and bread, Chiara for the congeniality, Sara D'Ag (Chiara's friend), Fabbrizio for the Lazial chorus, Liz for the smile, Leah for her Italian origins, Ten Tigers, Ornella, FAES coffe, Dafne, and her parties, Fra and the cakes, Luci and the poetry, Eli, Isla and Leor to be the best Juice in town. To Camille and Tiki, remembering Caaaaars. Thanks for the time we spent together, in sickness and in health.

Thanks to all of you and not you SARS-CoV-2!!!

# 7 REFERENCES


Alabi, A. A. and R. W. Tsien (2013). "Perspectives on kiss-and-run: role in exocytosis, endocytosis, and neurotransmission." Annu Rev Physiol **75**: 393-422.

Albillos, A., G. Dernick, H. Horstmann, W. Almers, G. Alvarez de Toledo and M. Lindau (1997). "The exocytotic event in chromaffin cells revealed by patch amperometry." Nature **389**(6650): 509-512.

Ales, E., L. Tabares, J. M. Poyato, V. Valero, M. Lindau and G. Alvarez de Toledo (1999). "High calcium concentrations shift the mode of exocytosis to the kiss-and-run mechanism." Nat Cell Biol **1**(1): 40-44.

Alvarez de Toledo, G., R. Fernandez-Chacon and J. M. Fernandez (1993). "Release of secretory products during transient vesicle fusion." Nature **363**(6429): 554-558.

Aunis, D. and M. F. Bader (1988). "The cytoskeleton as a barrier to exocytosis in secretory cells." J Exp Biol **139**: 253-266.

Bleckert, A., H. Photowala and S. Alford (2012). "Dual pools of actin at presynaptic terminals." J Neurophysiol **107**(12): 3479-3492.

Bloom, O., E. Evergren, N. Tomilin, O. Kjaerulff, P. Low, L. Brodin, V. A. Pieribone, P. Greengard and O. Shupliakov (2003). "Colocalization of synapsin and actin during synaptic vesicle recycling." J Cell Biol **161**(4): 737-747.

Bornstein, S. R., M. Ehrhart-Bornstein, A. Androutsellis-Theotokis, G. Eisenhofer, V. Vukicevic, J. Licinio, M. L. Wong, P. Calissano, G. Nistico, P. Preziosi and R. Levi-Montalcini (2012). "Chromaffin cells: the peripheral brain." Mol Psychiatry **17**(4): 354-358.

Brandt, B. L., S. Hagiwara, Y. Kidokoro and S. Miyazaki (1976). "Action potentials in the rat chromaffin cell and effects of acetylcholine." J Physiol **263**(3): 417-439.

Brodin, L. and O. Shupliakov (2006). "Giant reticulospinal synapse in lamprey: molecular links between active and periactive zones." Cell Tissue Res **326**(2): 301-310.

Ceccarelli, B., W. P. Hurlbut and A. Mauro (1973). "Turnover of transmitter and synaptic vesicles at the frog neuromuscular junction." J Cell Biol **57**(2): 499-524.

Chernomordik, L. V. and M. M. Kozlov (2008). "Mechanics of membrane fusion." Nat Struct Mol Biol **15**(7): 675-683.

Chiang, H. C., W. Shin, W. D. Zhao, E. Hamid, J. Sheng, M. Baydyuk, P. J. Wen, A. Jin, F. Momboisse and L. G. Wu (2014). "Post-fusion structural

changes and their roles in exocytosis and endocytosis of dense-core vesicles." Nat Commun **5**: 3356.

Clayton, E. L., G. J. Evans and M. A. Cousin (2008). "Bulk synaptic vesicle endocytosis is rapidly triggered during strong stimulation." J Neurosci **28**(26): 6627-6632.

Collins, A., A. Warrington, K. A. Taylor and T. Svitkina (2011). "Structural organization of the actin cytoskeleton at sites of clathrin-mediated endocytosis." Curr Biol **21**(14): 1167-1175.

Cooper, J. A. (1987). "Effects of cytochalasin and phalloidin on actin." J Cell Biol **105**(4): 1473-1478.

Dayel, M. J., E. A. Holleran and R. D. Mullins (2001). "Arp2/3 complex requires hydrolyzable ATP for nucleation of new actin filaments." Proceedings of the National Academy of Sciences **98**(26): 14871-14876.

Eltoum, I., J. Fredenburgh, R. B. Myers and W. E. Grizzle (2001). "Introduction to the Theory and Practice of Fixation of Tissues." Journal of Histotechnology **24**(3): 173-190.

Engqvist-Goldstein, A. E. and D. G. Drubin (2003). "Actin assembly and endocytosis: from yeast to mammals." Annu Rev Cell Dev Biol **19**: 287-332.

Evanko, D. (2009). "Fluorescent false neurotransmitters." Nature Methods **6**: 486.

Evergren, E., H. Gad, K. Walther, A. Sundborger, N. Tomilin and O. Shupliakov (2007). "Intersectin is a negative regulator of dynamin recruitment to the synaptic endocytic zone in the central synapse." J Neurosci **27**(2): 379-390.

Fesce, R., F. Grohovaz, F. Valtorta and J. Meldolesi (1994). "Neurotransmitter release: fusion or 'kiss-and-run'?" Trends Cell Biol **4**(1): 1-4.

Fifkova, E. and R. J. Delay (1982). "CYTOPLASMIC ACTIN IN NEURONAL PROCESSES AS A POSSIBLE MEDIATOR OF SYNAPTIC PLASTICITY." Journal of Cell Biology **95**(1): 345-350.

Gad, H., P. Low, E. Zotova, L. Brodin and O. Shupliakov (1998). "Dissociation between Ca2+-triggered synaptic vesicle exocytosis and clathrin-mediated endocytosis at a central synapse." Neuron **21**(3): 607-616.

Gonzalez-Jamett, A. M., F. Momboisse, M. J. Guerra, S. Ory, X. Baez-Matus, N. Barraza, V. Calco, S. Houy, E. Couve, A. Neely, A. D. Martinez, S. Gasman and A. M. Cardenas (2013). "Dynamin-2 regulates fusion pore expansion and quantal release through a mechanism that involves actin dynamics in neuroendocrine chromaffin cells." PLoS One **8**(8): e70638.

Grillner, S. (2003). "The motor infrastructure: from ion channels to neuronal networks." Nat Rev Neurosci **4**(7): 573-586.

He, L., X. S. Wu, R. Mohan and L. G. Wu (2006). "Two modes of fusion pore opening revealed by cell-attached recordings at a synapse." Nature **444**(7115): 102-105.

Heuser, J. E. and T. S. Reese (1973). "EVIDENCE FOR RECYCLING OF SYNAPTIC VESICLE MEMBRANE DURING TRANSMITTER RELEASE AT THE FROG NEUROMUSCULAR JUNCTION." The Journal of Cell Biology **57**(2): 315-344.

Heuser, J. E. and T. S. Reese (1981). "Structural changes after transmitter release at the frog neuromuscular junction." J Cell Biol **88**(3): 564-580.

Hirokawa, N. and J. E. Heuser (1981). "Quick-freeze, deep-etch visualization of the cytoskeleton beneath surface differentiations of intestinal epithelial cells." J Cell Biol **91**(2 Pt 1): 399-409.

Hroudova, J., N. Singh and Z. Fisar (2014). "Mitochondrial dysfunctions in neurodegenerative diseases: relevance to Alzheimer's disease." Biomed Res Int **2014**: 175062.

Jacobson, D. A. and L. H. Philipson (2007). "Action potentials and insulin secretion: new insights into the role of Kv channels." Diabetes Obes Metab **9 Suppl 2**: 89-98.

Jenkins, T. A., J. C. Nguyen, K. E. Polglaze and P. P. Bertrand (2016). "Influence of Tryptophan and Serotonin on Mood and Cognition with a Possible Role of the Gut-Brain Axis." Nutrients **8**(1).

Kaksonen, M. and A. Roux (2018). "Mechanisms of clathrin-mediated endocytosis." Nat Rev Mol Cell Biol **19**(5): 313-326.

Kasprowicz, J., S. Kuenen, K. Miskiewicz, R. L. Habets, L. Smitz and P. Verstreken (2008). "Inactivation of clathrin heavy chain inhibits synaptic recycling but allows bulk membrane uptake." J Cell Biol **182**(5): 1007-1016.

Klyachko, V. A. and M. B. Jackson (2002). "Capacitance steps and fusion pores of small and large-dense-core vesicles in nerve terminals." Nature **418**(6893): 89-92.

Kononenko, N. L. and V. Haucke (2015). "Molecular mechanisms of presynaptic membrane retrieval and synaptic vesicle reformation." Neuron **85**(3): 484-496.

Korobova, F. and T. Svitkina (2010). "Molecular architecture of synaptic actin cytoskeleton in hippocampal neurons reveals a mechanism of dendritic spine morphogenesis." Mol Biol Cell **21**(1): 165-176.

Kozlov, M. M. and L. V. Chernomordik (2015). "Membrane tension and membrane fusion." Curr Opin Struct Biol **33**: 61-67.

Landis, D. M. D., A. K. Hall, L. A. Weinstein and T. S. Reese (1988). "The organization of cytoplasm at the presynaptic active zone of a central nervous system synapse." Neuron **1**(3): 201-209.

Li, Y. C., W. Z. Bai, L. Zhou, L. K. Sun and T. Hashikawa (2010). "Nonhomogeneous distribution of filamentous actin in the presynaptic terminals on the spinal motoneurons." J Comp Neurol **518**(16): 3184-3192.

Lian, G. and V. L. Sheen (2015). "Cytoskeletal proteins in cortical development and disease: actin associated proteins in periventricular heterotopia." Front Cell Neurosci **9**: 99.

Lindau, M. and G. Alvarez de Toledo (2003). "The fusion pore." Biochim Biophys Acta **1641**(2-3): 167-173.

Lomasney, J. W., H. F. Cheng, L. P. Wang, Y. Kuan, S. Liu, S. W. Fesik and K. King (1996). "Phosphatidylinositol 4,5-bisphosphate binding to the pleckstrin homology domain of phospholipase C-delta1 enhances enzyme activity." J Biol Chem **271**(41): 25316-25326.

Mastronarde, D. N. (2005). "Automated electron microscope tomography using robust prediction of specimen movements." Journal of Structural Biology **152**(1): 36-51.

Miller, T. M. and J. E. Heuser (1984). "Endocytosis of synaptic vesicle membrane at the frog neuromuscular junction." J Cell Biol **98**(2): 685-698.

Morales, M., M. A. Colicos and Y. Goda (2000). "Actin-Dependent Regulation of Neurotransmitter Release at Central Synapses." Neuron **27**(3): 539-550.

Nakata, T. and N. Hirokawa (1987). "Cytoskeletal reorganization of human platelets after stimulation revealed by the quick-freeze deep-etch technique." J Cell Biol **105**(4): 1771-1780.

Nemoto, T., T. Kojima, A. Oshima, H. Bito and H. Kasai (2004). "Stabilization of exocytosis by dynamic F-actin coating of zymogen granules in pancreatic acini." J Biol Chem **279**(36): 37544-37550.

Nightingale, T. D., I. J. White, E. L. Doyle, M. Turmaine, K. J. Harrison-Lavoie, K. F. Webb, L. P. Cramer and D. F. Cutler (2011). "Actomyosin II contractility expels von Willebrand factor from Weibel-Palade bodies during exocytosis." J Cell Biol **194**(4): 613-629.

O'Connor, D. T., S. K. Mahata, M. Mahata, Q. Jiang, V. Y. Hook and L. Taupenot (2007). "Primary culture of bovine chromaffin cells." Nat Protoc **2**(5): 1248-1253.

Olivares, M. J., A. M. Gonzalez-Jamett, M. J. Guerra, X. Baez-Matus, V. Haro-Acuna, N. Martinez-Quiles and A. M. Cardenas (2014). "Src kinases regulate de novo actin polymerization during exocytosis in neuroendocrine chromaffin cells." PLoS One **9**(6): e99001.

Pearse, B. M. (1975). "Coated vesicles from pig brain: purification and biochemical characterization." J Mol Biol **97**(1): 93-98.

Pearse, B. M. (1976). "Clathrin: a unique protein associated with intracellular transfer of membrane by coated vesicles." Proc Natl Acad Sci U S A **73**(4): 1255-1259.

Pilo Boyl, P., A. Di Nardo, C. Mulle, M. Sassoe-Pognetto, P. Panzanelli, A. Mele, M. Kneussel, V. Costantini, E. Perlas, M. Massimi, H. Vara, M. Giustetto and W. Witke (2007). "Profilin2 contributes to synaptic vesicle exocytosis, neuronal excitability, and novelty-seeking behavior." EMBO J **26**(12): 2991-3002.

Richards, D. A., S. O. Rizzoli and W. J. Betz (2004). "Effects of wortmannin and latrunculin A on slow endocytosis at the frog neuromuscular junction." J Physiol **557**(Pt 1): 77-91.

Rorsman, P. and M. Braun (2013). "Regulation of insulin secretion in human pancreatic islets." Annu Rev Physiol **75**: 155-179.

Sablin, E. P., J. F. Dawson, M. S. VanLoock, J. A. Spudich, E. H. Egelman and R. J. Fletterick (2002). "How does ATP hydrolysis control actin's associations?" Proceedings of the National Academy of Sciences **99**(17): 10945-10947.

Sankaranarayanan, S., P. P. Atluri and T. A. Ryan (2003). "Actin has a molecular scaffolding, not propulsive, role in presynaptic function." Nat Neurosci **6**(2): 127-135.

Schindelin, J., I. Arganda-Carreras, E. Frise, V. Kaynig, M. Longair, T. Pietzsch, S. Preibisch, C. Rueden, S. Saalfeld, B. Schmid, J. Y. Tinevez, D. J. White, V. Hartenstein, K. Eliceiri, P. Tomancak and A. Cardona (2012). "Fiji: an open-source platform for biological-image analysis." Nat Methods **9**(7): 676-682.

Schober, A., R. Parlato, K. Huber, R. Kinscherf, B. Hartleben, T. B. Huber, G. Schutz and K. Unsicker (2013). "Cell loss and autophagy in the extra-adrenal chromaffin organ of Zuckerkandl are regulated by glucocorticoid signalling." J Neuroendocrinol **25**(1): 34-47.

Shupliakov, O., O. Bloom, J. S. Gustafsson, O. Kjaerulff, P. Löw, N. Tomilin, V. A. Pieribone, P. Greengard and L. Brodin (2002). "Impaired recycling of synaptic vesicles after acute perturbation of the presynaptic actin cytoskeleton." Proceedings of the National Academy of Sciences **99**(22): 14476-14481.

Shupliakov, O., P. Low, D. Grabs, H. Gad, H. Chen, C. David, K. Takei, P. De Camilli and L. Brodin (1997). "Synaptic vesicle endocytosis impaired by disruption of dynamin-SH3 domain interactions." Science **276**(5310): 259-263.

Smythe, E. and K. R. Ayscough (2006). "Actin regulation in endocytosis." J Cell Sci **119**(Pt 22): 4589-4598.

Sochacki, K. A., A. M. Dickey, M. P. Strub and J. W. Taraska (2017). "Endocytic proteins are partitioned at the edge of the clathrin lattice in mammalian cells." Nat Cell Biol **19**(4): 352-361.

Sochacki, K. A., B. T. Larson, D. C. Sengupta, M. P. Daniels, G. Shtengel, H. F. Hess and J. W. Taraska (2012). "Imaging the post-fusion release and capture of a vesicle membrane protein." Nat Commun **3**: 1154.

Sochacki, K. A., G. Shtengel, S. B. van Engelenburg, H. F. Hess and J. W. Taraska (2014). "Correlative super-resolution fluorescence and metal-replica transmission electron microscopy." Nature Methods **11**(3): 305-U278.

Sokac, A. M., C. Co, J. Taunton and W. Bement (2003). "Cdc42-dependent actin polymerization during compensatory endocytosis in Xenopus eggs." Nat Cell Biol **5**(8): 727-732.

Spector, I., N. R. Shochet, D. Blasberger and Y. Kashman (1989). "Latrunculins--novel marine macrolides that disrupt microfilament organization and affect cell growth: I. Comparison with cytochalasin D." Cell Motil Cytoskeleton **13**(3): 127-144.

Sudhof, T. C. (2004). "The synaptic vesicle cycle." Annu Rev Neurosci **27**: 509-547.

Takei, K., O. Mundigl, L. Daniell and P. De Camilli (1996). "The synaptic vesicle cycle: a single vesicle budding step involving clathrin and dynamin." J Cell Biol **133**(6): 1237-1250.

Taraska, J. W., D. Perrais, M. Ohara-Imaizumi, S. Nagamatsu and W. Almers (2003). "Secretory granules are recaptured largely intact after stimulated exocytosis in cultured endocrine cells." Proc Natl Acad Sci U S A **100**(4): 2070-2075.

Thiele, C., M. J. Hannah, F. Fahrenholz and W. B. Huttner (2000). "Cholesterol binds to synaptophysin and is required for biogenesis of synaptic vesicles." Nat Cell Biol **2**(1): 42-49.

Trouillon, R. and A. G. Ewing (2014). "Actin controls the vesicular fraction of dopamine released during extended kiss and run exocytosis." ACS Chem Biol **9**(3): 812-820.

Vitale, M. L., E. P. Seward and J. M. Trifaro (1995). "Chromaffin cell cortical actin network dynamics control the size of the release-ready vesicle pool and the initial rate of exocytosis." Neuron **14**(2): 353-363.

Watanabe, S., B. R. Rost, M. Camacho-Perez, M. W. Davis, B. Sohl-Kielczynski, C. Rosenmund and E. M. Jorgensen (2013). "Ultrafast endocytosis at mouse hippocampal synapses." Nature **504**(7479): 242-247.

Watanabe, S., T. Trimbuch, M. Camacho-Perez, B. R. Rost, B. Brokowski, B. Sohl-Kielczynski, A. Felies, M. W. Davis, C. Rosenmund and E. M.

Jorgensen (2014). "Clathrin regenerates synaptic vesicles from endosomes." Nature **515**(7526): 228-233.

Wen, P. J., S. Grenklo, G. Arpino, X. Tan, H. S. Liao, J. Heureaux, S. Y. Peng, H. C. Chiang, E. Hamid, W. D. Zhao, W. Shin, T. Nareoja, E. Evergren, Y. Jin, R. Karlsson, S. N. Ebert, A. Jin, A. P. Liu, O. Shupliakov and L. G. Wu (2016). "Actin dynamics provides membrane tension to merge fusing vesicles into the plasma membrane." Nat Commun **7**: 12604.

Winkler, H. (1993). "The adrenal chromaffin granule: a model for large dense core vesicles of endocrine and nervous tissue." J Anat **183 ( Pt 2)**: 237-252.

Wolf, M., A. M. Zimmermann, A. Gorlich, C. B. Gurniak, M. Sassoe-Pognetto, E. Friauf, W. Witke and M. B. Rust (2015). "ADF/Cofilin Controls Synaptic Actin Dynamics and Regulates Synaptic Vesicle Mobilization and Exocytosis." Cereb Cortex **25**(9): 2863-2875.

Wu, L. G., E. Hamid, W. Shin and H. C. Chiang (2014). "Exocytosis and endocytosis: modes, functions, and coupling mechanisms." Annu Rev Physiol **76**: 301-331.

Wu, W. and L. G. Wu (2007). "Rapid bulk endocytosis and its kinetics of fission pore closure at a central synapse." Proc Natl Acad Sci U S A **104**(24): 10234-10239.

Wu, X. S., S. H. Lee, J. Sheng, Z. Zhang, W. D. Zhao, D. Wang, Y. Jin, P. Charnay, J. M. Ervasti and L. G. Wu (2016). "Actin Is Crucial for All Kinetically Distinguishable Forms of Endocytosis at Synapses." Neuron.

Xu, Y., S. W. Zhu and Q. W. Li (2016). "Lamprey: a model for vertebrate evolutionary research." Zool Res **37**(5): 263-269.

Zhang, B., Y. H. Koh, R. B. Beckstead, V. Budnik, B. Ganetzky and H. J. Bellen (1998). "Synaptic vesicle size and number are regulated by a clathrin adaptor protein required for endocytosis." Neuron **21**(6): 1465-1475.

Zhao, W. D., E. Hamid, W. Shin, P. J. Wen, E. S. Krystofiak, S. A. Villarreal, H. C. Chiang, B. Kachar and L. G. Wu (2016). "Hemi-fused structure mediates and controls fusion and fission in live cells." Nature **534**(7608): 548-552.